Optimal Configuration of Renewable Energy DGs Based on Improved Northern Goshawk Optimization Algorithm Considering Load and Generation Uncertainties

Gonggui Chen, Jiajie Li, Yuansen Xu, Bo Peng, Hao Tan and Hongyu Long*

Abstract—**This paper proposes a distributed generator (DG) optimization framework based on an improved northern goshawk optimization (INGO) algorithm to install multiple DGs into the distributed system (DS) simultaneously. Various case studies are conducted in constant or varying load and generation models. The framework considers the power system's critical constraints while optimizing each DG's location, capacity, and power factor to minimize energy losses and voltage deviations and improve DG penetration levels and system voltage distribution. The effectiveness and stability of the INGO algorithm were first verified in two constant test systems, and the effect of the optimal power factor of the DG on the system was considered. The results of all case studies show that the INGO algorithm performs better than other existing methods in reducing active power losses and voltage deviations. When the three parameters of generator location, capacity, and power factor were optimized simultaneously, the active power losses of the two test systems were reduced by 93.96% and 98.11%, respectively. On this basis, photovoltaics (PVs) and wind turbines (WTs) as renewable energy DGs (REDGs) were also introduced in two changing test systems. The performance gap between two REDGs and conventional generators (CGs) is compared. The all-day active energy losses in the two tested systems were reduced by 88.27% and 94.74% after WTs installation. Much higher than 51.23% and 53.64% after installing PVs, almost as good as installing CGs. Therefore, WTs can replace CGs to reduce carbon emissions because the difference in energy loss and voltage deviation between the two is tiny.**

Index Terms—**Distributed generator, power factor, energy loss, carbon emissions, distributed system**

Manuscript received October 2, 2022; revised February 28, 2023.

Gonggui Chen is a professor at Key Laboratory of Industrial Internet of Things and Networked Control, Ministry of Education, Chongqing University of Posts and Telecommunications, Chongqing 400065, China; (e-mail: chenggpower@ 126.com).

Jiajie Li is a graduate student of Chongqing University of Posts and Telecommunications, Chongqing 400065, China (e-mail: chinalijiajie@163.com).

Yuansen Xu is an engineer at the Economic and Technology Research Institute, State Grid Chongqing Electric Power Company, Chongqing 401120, China(e-mail: yuansenxu_cq@163.com).

Bo Peng is a senior engineer at the Economic and Technology Research Institute, State Grid Chongqing Electric Power Company, Chongqing 401120, China(e-mail: bopeng_cq@163.com).

Hao Tan is a senior engineer at the Economic and Technology Research Institute, State Grid Chongqing Electric Power Company, Chongqing 401120, China (e-mail: tanhao_cq@163.com).

Hongyu Long* is a professor-level senior engineer of Chongqing Key Laboratory of Complex Systems and Bionic Control, Chongqing University of Posts and Telecommunications, Chongqing 400065, China (corresponding author to provide phone: +8613996108500; e-mail: longhongyu20@163.com).

I. Introduction

With the increasing load demand and the transmission of electrical energy on long transmission and distribution lines, the distribution network faces many challenges, such as increased power loss, poor voltage regulation, and poor power quality. These problems harm the power system's performance and the power supply's reliability [1]. Modern power systems focus more on distributed generation than traditional centralized generation because distributed generation positively affects the distribution system's planning and operation. Unlike a conventional generator, distributed generator (DG) is referred to as a small generating set, with a capacity size of 1kW to 50MW, and is located closer to the customer. Generators of either conventional (including micro-turbines, gas turbines, diesel engines, and fuel cells) or renewable energy (such as photovoltaics and wind turbines) might be considered DGs [2]. The greenhouse effect has grown more pronounced in recent years due to global warming. CGs emit many greenhouse emissions in the energy sector. In contrast, REDGs are clean, low-carbon generators with minimal pollution [3].

Despite the environmental benefits, the installation effects of DGs must be carefully evaluated when installing REDGs in a DS. These resources are intermittent, and weather conditions significantly impact them [4]. With only centralized generation, the DS's load flow is from the substation to the customer, while with the installation of DG, the DS's load flow is bi-directional. Inadequate DG planning may result in under or over-generation, worsening power quality metrics, and other issues [5]. When DG is appropriately configured, all relevant parameters are improved, and power loss and carbon emissions are reduced. Many different DG optimization techniques have been proposed to effectively solve the problem of optimal distributed generator allocation (ODGA).

Analytical approaches have been used in some research to address the ODGA problem. In [6], four new analytical methods are proposed to determine the optimal siting and sizing of DGs to reduce the system's power loss. In [7], a model with a two-level framework combination is proposed. The first step of this model is to determine the location of the DG based on the sensitivity index, and the second step is to calculate the capacity of the DG based on the proposed analytical expression. In general, the analytical approach has a short computation time and is easy to handle simple ODGA problems. However, as the number and types of installed DGs increase, the ODGA problem will become

more complex, posing a significant challenge to the analytical method.

An alternative approach to solve the ODGA problem is to use an artificial intelligence-based method. The artificial intelligence-based approach is highly spontaneous, easy to implement, and can solve complex ODGA problems. In [8], the krill herd algorithm (KHA) method is proposed to minimize the system's active power and energy loss. The authors of [9-11] propose an improved equilibrium optimization algorithm (IEOA), an enhanced gravitational search algorithm (EGSA), and a chaotic search group algorithm (CSGA) for simultaneously reconfiguring the distributed feeders and optimally allocating the DGs in order to minimize active power loss and maximize the voltage stability index of the DS. In [12-14], the sensitivity coefficient is first used to determine the candidate bus locations of DGs. Then, Particle Swarm Optimization (PSO), Improved Butterfly Algorithm (IBA), and Ant Lion Optimizer (ALO) algorithms are used to determine the optimal capacity of DGs, respectively, which reduces the algorithm's search space and active power loss.

In addition, the optimization model can also solve the multi-objective ODGA problem. Regarding the multi-objective framework, two techniques, the weighting method [15] and Pareto-front-based optimization [16-18], have been used in most studies. Ref. [19] utilizes a modified Imperialistic Competitive Algorithm (ICA) form and considers the load variation, which varies linearly from the essential 50% to 150% (1% increase at a time); finally, it results in a general expression for the capacity variation of DG with the load.

Besides single algorithms, many hybrid algorithms have been proposed to solve ODGA problems. The hybrid algorithm retains the advantages of the single algorithm and improves convergence speed and accuracy. In [20-25], beetle antennae search algorithm (BASA), genetic algorithm (GA), shuffled frog leap algorithm (SLFA), crow search algorithm (CSA), and analytic method are respectively combined with PSO for solving single-objective or multi-objective ODGA problems. In [26], a methodology based on symbiosis organism search and neural network algorithm (SOS-NNA) is proposed to configure DG and capacitors simultaneously.

Most studies only considered DGs operating at unity power factor (UPF) and predefined power factor, ignoring the effect of optimal power factor (OPF) on the performance of DGs. Only in [27-31] have researchers examined the effect of DG operated at OPF on the performance parameters of DS. Ref. [30] also considers the effect of the optimal number of DGs on the performance parameters of DS, and "dispatchable" power factors for each period in a given range are proposed in smart grid schemes to minimize the reactive power loss.

In most cases, DG studies are performed with constant power and load models, which are not applicable in practical DS. In addition, the optimal location and capacity of the DG at peak load are not necessarily the same as at other load levels [32]. In [33], the load variation of DS and the intermittent output power of DG are considered essential factors in assessing the impact of DG on the grid.

Synthesizing the above literature, in some studies, the candidate locations of DG are usually selected based on the sensitivity factor, which leads to a significant reduction of the search space but eliminates the locations of certain potential candidate buses. In addition, most of the above studies need to examine well the impact of the optimal power factor of DG on the network performance. Studies of the ODGA problem usually consider only constant generation and constant load models and rarely consider variable generation and variable load models.

This research offers an optimization framework for DGs based on the INGO algorithm to simultaneously optimize numerous DGs' locations, capacities, and power factors in the DS. In addition, the performance of the proposed algorithm is assessed under the simultaneous changes in load and generation.

The main contributions of this paper are as follows: (i) The effects of different DG's power factors on the network performance are considered, and the optimal setting of the DG's power factor is investigated. (ii) The uncertainty of load and generation is considered, and the total time is 24 hours. (iii)The original NGO algorithm is improved and applied to the ODGA problem for comparison. (iv) High-penetration REDGs are optimally configured in the DS, which can significantly reduce carbon emissions. (v) PVs and WTs, regarded as REDGs, are optimally configured in the DS. The results are compared with the configuration of CGs to select the best solution for replacing CGs with REDGs. (vi) PV works not only at UPF as in previous literature but also at OPF according to the latest standard IEEE1547 [26], which is a novel study.

The rest of the paper is structured as follows. Section II presents the mathematical expressions of the ODGA problem. Section III details the proposed INGO algorithm's definition and application steps and verifies the improved algorithm's effectiveness in four benchmark functions. In Section IV, the optimal configuration of DGs is performed under two different load and generation scenarios and simulated in 33-bus and 69-bus radial distributed networks (RDNs), respectively. Then the simulation results of all studied cases are compared to verify the effectiveness of the proposed optimization framework in solving the ODGA problem. Finally, the paper is summarized in Section V.

II. Problem Formulations

The ODGA problem refers to the rational allocation of DG location, capacity, and power factor in the DS to make the whole DS operate in a stable and economic state. The ODGA problem contains several optimization objectives and system constraints. This section gives seven objective functions, including instantaneous active and reactive power loss, instantaneous voltage deviation, daily active and reactive energy loss, daily voltage deviation, and DG's penetration level. The constraints of the ODGA problem are described from three aspects: power balance constraints, DG's constraints, and voltage and current constraints.

A. Objective functions

The power system's active and reactive power loss is calculated as shown in (1) and (2).

$$P_{loss,t} = \sum_{i=1}^{NL} \{(I_{i,t})^2 \times R_i\} \tag{1}$$

$$Q_{loss,t} = \sum_{i=1}^{NL} \{(I_{i,t})^2 \times X_i\} \tag{2}$$

where, $P_{loss,t}$ denotes the total active power loss of the system at time t in kW; $Q_{loss,t}$ denotes the total reactive power loss of the system at time t in kVAr; $I_{i,t}$ denotes the

current value of the i^{th} branch at time t in kA; NL is the total number of branches of the system, and R_i and X_i represent the resistance and reactance values of the i^{th} branch in Ω, respectively.

The active and reactive energy loss for period Δt is calculated using (3) and (4), respectively [34].

$$EL_P = P_{loss,\Delta t} \times \Delta t \tag{3}$$

$$EL_Q = Q_{loss,\Delta t} \times \Delta t \tag{4}$$

where, EL_P is the active energy loss in kWh; EL_Q is the reactive energy loss in kVArh.

Considering the hourly load variation (Δt = 1 hour), the total daily active energy loss and total daily reactive energy loss are calculated as shown in (5) and (6).

$$DEL_P = \sum_{t=1}^{24} P_{loss,t} \tag{5}$$

$$DEL_Q = \sum_{t=1}^{24} Q_{loss,t} \tag{6}$$

where, DEL_P is the total daily active energy loss in kWh and DEL_Q is the total daily reactive energy loss in kVArh.

The voltage deviation indicates how close each bus's actual voltage is to the system's nominal voltage, and the calculation formula is shown in (7).

$$VD^t = \sum_{i=1}^{NB} (V_{i,t} - V_{ref})^2 \tag{7}$$

where, VD^t denotes the voltage deviation of the system at moment t, NB denotes the total number of buses of the system, $V_{i,t}$ denotes the voltage magnitude of bus i at moment t, and V_{ref} denotes the voltage magnitude of the reference bus, which is set to 1 p.u here.

The daily total voltage deviation (DVD), considering the average daily load variation, is calculated as shown in (8).

$$DVD = \sum_{t=1}^{24} VD^t \tag{8}$$

The formula for calculating DG's penetration level (pl) is shown in (9).

$$pl(\%) = \frac{S_{DG}}{S_{Load} + S_{loss}} \times 100 \tag{9}$$

where, S_{DG} denotes the apparent power generated by DG, S_{Load} denotes the apparent power of the total system load, and S_{loss} denotes the loss of apparent power of the system.

The objective of the ODGA problem is to maximize the positive impacts and minimize the adverse effects on the power system. This paper's objective functions are minimizing instantaneous active power loss and daily active energy loss, as shown in (10) and (11).

$$OF_1 = \min(P_{loss}) \tag{10}$$

$$OF_2 = \min(DEL_P) \tag{11}$$

B. Constraints

a: Power balance constraints

The total power generated in the power system is equal to the sum of the load's power and the lost power, and the expressions are shown in (12) and (13).

$$P_{\inf eed} + \sum_{i=1}^{N_{DG}} P_{DG,i} = P_D + P_{loss} \tag{12}$$

$$Q_{\inf eed} + \sum_{i=1}^{N_{DG}} Q_{DG,i} = Q_D + Q_{loss} \tag{13}$$

where, N_{DG} is the number of DGs; P_{infeed} and Q_{infeed} are the active and reactive power injected into DS by the substation, respectively; $P_{DG,i}$ and $Q_{DG,i}$ are the active and reactive power generated by the i^{th} DG, respectively; P_D and Q_D are the total active and reactive power of the load, respectively.

b: Voltage and current constraints

$$0.9\,p.u \le V_i \le 1.05\,p.u, \forall i \in 1,2,\ldots,NB \tag{14}$$

$$|I_k| \le |I_{\max,k}|, k = 1,2,\ldots,NL \tag{15}$$

c: Constraints of DG

The output power of each DG is limited by the load power of the test network, as shown in (16) and (17) [35].

$$0 \le P_{DG,i} \le P_{Load,\max}, \forall i \in 1,2,\ldots,N_{DG} \tag{16}$$

$$0 \le Q_{DG,i} \le Q_{Load,\max}, \forall i \in 1,2,\ldots,N_{DG} \tag{17}$$

The position of DG cannot be on the same bus and reference bus, defined as follows.

$$2 \le L_{DG,i} \ne L_{DG,j} \le NB \tag{18}$$

where, $L_{DG,i}$ and $L_{DG,j}$ denote the location of the i^{th} DG and j^{th} DG, respectively.

In the present study, the power factor of each DG is limited to between 0.8 and unity.

$$0.8 \le pf_{DG,i} \le 1, \forall i \in 1,2,\ldots,N_{DG} \tag{19}$$

III. Algorithm Improvement

Meta-heuristic algorithms can provide sufficiently good solutions to large-scale optimization problems in an acceptable amount of time, especially when information is incomplete or computational power is limited. The population intelligence optimization algorithm belongs to one of the biological heuristics. Its outstanding feature is that it utilizes population intelligence to perform a collaborative search to find the optimal solution in the solution space. This paper uses the Northern Goshawk Optimization (NGO) algorithm to achieve the optimal allocation of DGs.

A. Northern Goshawk Optimization (NGO)

The Northern Goshawk Optimization (NGO) algorithm is a population optimization algorithm proposed in 2022 by Mohammad Dehghani [36]. The algorithm simulates the behaviour of the northern goshawk during hunting. The NGO algorithm divides the northern goshawk's hunting process into two phases: prey recognition with an attack (exploration phase) and pursuit with escape (exploitation phase). Balancing global exploration and local search stages can efficiently tackle practical engineering design optimization difficulties.

a: NGO algorithm initialization process

In the NGO algorithm, each individual in the population represents a solution to the problem. From a mathematical point of view, each individual is a vector, and the user should predefine the dimension of each vector (denoted as D). Its value should be equal to the value of the control variable. For example, to optimize the location, capacity, and power factor of 3 DGs, D should be set to 9. When the population size is set to N, the population matrix P is depicted as shown in (20).

$$P = [X_1, X_2, \ldots, X_N]; X_i = [x_{i1}, x_{i2}, \ldots x_{iD}] \tag{20}$$

At the beginning of the algorithm, the 3 DGs are initialized with the first three parameters of each individual indicating the location of the DGs, the following three parameters indicating the capacity of the DGs, and the last

three parameters indicating the power factor of the DGs.

b: Phase I: prey identification and attack (exploration)

This phase performs a global search of the search space to determine the optimal region. The mathematical model of the first stage is shown in equations (21) to (23).

$$P_i = X_k, i = 1,2,\ldots,N, k = 1,2,...,i-1,i+1,...,N \quad (21)$$

$$x_{i,j,new1} = \begin{cases} x_{i,j} + r(P_{i,j} - Ix_{i,j}), F_{Pi} < F_i \\ x_{i,j} + r(x_{i,j} - P_{i,j}), F_{Pi} \geq F_i \end{cases} \quad (22)$$

$$X_{i1} = \begin{cases} X_{i,new1}, F_{i,new1} < F_i \\ X_i, F_{i,new1} \geq F_i \end{cases} \quad (23)$$

where, P_i is the location of the k^{th} northern goshawk's prey, F_{Pi} is its objective function value, and k is a random integer in the range [1, N]. $X_{i,new1}$ is the new position of the i^{th} northern goshawk; $x_{i,j,new1}$ is the new position of the j^{th} dimension of the i^{th} northern goshawk; $F_{i,new1}$ is the updated objective function value for the i^{th} northern goshawk; X_{i1} is the i^{th} prey position determined by comparing the value of the objective function before and after the update of the i^{th} individual; r is a random number in the range [0,1]; I is a random integer equal to 1 or 2. Random numbers r and I generate random NGO behaviours in the search and update.

c: Phase II: chase and escape operation (exploitation)

This phase demonstrates the local search capability of the NGO algorithm for the search space. Assuming that the local search is performed within a radius of R, (24) to (26) show the mathematical expressions of the second stage.

$$x_{i,j,new2} = x_{i,j} + R(2r-1)x_{i,j} \quad (24)$$

$$R = 0.02\left(1 - \frac{t}{T}\right) \quad (25)$$

$$X_{i2} = \begin{cases} X_{i,new2}, F_{i,new2} < F_i \\ X_i, F_{i,new2} \geq F_i \end{cases} \quad (26)$$

where, t is the current iterations, and T is the maximum number of iterations.

B. Improved Northern Goshawk Optimization (INGO)

a: Improvement of the hunting process

In the hunting process of the NGO algorithm, the prey location update relies on the current prey location, and the positive impact of the individual optimal site of the prey on the search capability of the algorithm is not considered. To improve the search performance of the algorithm, inspired by the particle swarm optimization algorithm, the individual optimal position *Pbest* is introduced into the NGO algorithm to update the position of the prey.

$$x_{i,j,new1} = \begin{cases} Pbest_{i,j} + r(P_i - I * Pbest_{i,j}), F_{Pi} < F_i \\ Pbest_{i,j} + r(Pbest_{i,j} - P_i), F_{Pi} \geq F_i \end{cases} \quad (27)$$

$$x_{i,j,new2} = Pbest_{i,j} + R(2r-1)Pbest_{i,j} \quad (28)$$

where, $Pbest_{i,j}$ denotes the current optimal position of the j^{th} dimension of the i^{th} individual.

b: Priority processing constraints method

There are many control and state variables to deal with in this study, and it is challenging to ensure that all variables are within the constraints by simply comparing the magnitude of the objective function values. The prioritize constraints approach is developed to avoid having some variables outside the constraints, ensuring that the power system always functions in a steady state. The highest adoption priority is given to solutions that do not violate the constraints, a higher adoption priority is given to solutions that violate smaller constraints, and the lowest is given to solutions that violate the enormous constraints. The specific constraint-handling strategy is as follows.

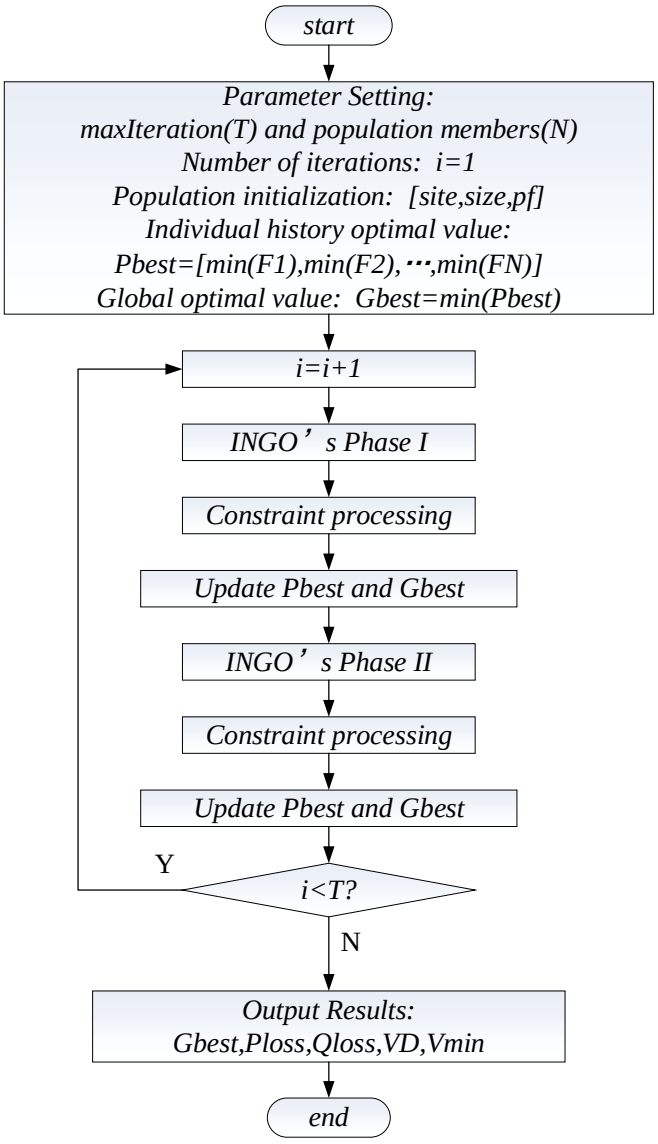

Fig. 1. Flow diagram of INGO algorithm

After updating the position, the j^{th} control variable of the i^{th} individual can be adjusted according to (29) if it is out of the constraint range.

$$x_{i,j,new} = \begin{cases} x_{i,j,new}^{\max}, if \quad x_{i,j,new} > x_{i,j,new}^{\max} \\ x_{i,j,new}^{\min}, if \quad x_{i,j,new} < x_{i,j,new}^{\min} \end{cases} \quad (29)$$

where, $x_{i,j,new}$ denotes the updated position of the j^{th} control variable for the i^{th} individual.

The handling of state variables that violate the constraints differs from control variables, and the constraint priority is used to handle the non-conforming state variables. The methods are shown in (30).

$$c_{i,j,new} = \begin{cases} u_{i,j,new} - u_{i,j,new}^{\max}, if \quad u_{i,j,new} > u_{i,j,new}^{\max} \\ u_{i,j,new}^{\min} - u_{i,j,new}, if \quad u_{i,j,new} < u_{i,j,new}^{\min} \\ 0, if \quad u_{i,j,new}^{\min} \leq u_{i,j,new} \leq u_{i,j,new}^{\max} \end{cases} \quad (30)$$

where, $u_{i,j,new}$ denotes the j^{th} state variable after the i^{th}

individual position update, and $c_{i,j,new}$ represents the constraint value it violates.

$$C_{i,new} = c_{i,1,new} + c_{i,2,new} + \cdots + c_{i,M,new} \tag{31}$$

where, $C_{i,new}$ denotes the sum of the state variable constraint violations after the i^{th} individual position update, and M is the number of state variables whose constraints are violated.

$$X_{inew} = \begin{cases} X_i, C_{i,new} > C_i \\ X_{i,new}, C_{i,new} < C_i \\ X_i, C_{i,new} = C_i \ and \ F_{i,new} \geq F_i \\ X_{i,new}, C_{i,new} = C_i \ and \ F_{i,new} < F_i \end{cases} \tag{32}$$

where, C_i denotes the total value of the state variable constraint violation before the i^{th} individual position update, F_i and $F_{i,new}$ represent the objective function values before and after the position update, respectively, and X_i and $X_{i,new}$ denote the positions before and after the update.

The INGO algorithm is applied to the ODGA problem, and the simplified flow chart is shown in Fig. 1.

C. Performance testing of algorithms

Six benchmark functions are utilized to test the effectiveness and rationality of the proposed INGO algorithm, and the NGO algorithm and PSO algorithm are introduced as comparative experiments. The integrated parameter settings of the six benchmark functions are shown in TABLE I. The dimensionality of the control variables for the six test functions is 30, the number of populations is 50, and the maximum number of iterations is 500. Each algorithm is tested thirty times for various test functions, with the best outcome used for comparison. The convergence curves of the six tested functions are shown in Fig. 2. As shown in Fig. 2, the INGO algorithm's convergence speed and convergence accuracy are better than the other two algorithms among the six tested functions. TABLE II shows the experimental results of the three algorithms for the six tested functions. The experimental results show that the INGO algorithm obtains better solutions than the NGO and PSO algorithms. In summary, the improved algorithm proposed in this paper is effective and feasible.

IV. Experimentation and Analysis

Two common RDNs, including the IEEE 33-bus and IEEE 69-bus, have been used to test the performance of the proposed INGO algorithm. Both test networks are applied to the model with constant or varied load and generation. Unity and optimal power factor scenarios are considered for the configuration study of DGs under each model. In the constant model， to evaluate the effectiveness of the proposed INGO algorithm, the initial NGO algorithm is also applied to solve the same problem, and the results are compared. The INGO and NGO algorithms are tested 30 times independently for each test case to obtain the best results.

A. Case study 1: Constant load and generation

a: The IEEE 33-bus network

The first test network is the standard IEEE small-scale RDN with 33 buses and 32 branches. Fig. 3 displays a single-line diagram of the small DS. At peak load, the total active and reactive loads are 3.715 MW and 2.3 MVAr at the base values of 100 MVA and 12.66 kV, respectively. The test network's load and line data are provided in [37]. The active network loss and reactive network loss of the system without DG installation are 211 kW and 143.13 kVAr, respectively, according to the results of the tide calculation at peak load. Fig. 4 displays the voltage magnitude of each bus, and the system voltage deviation is 0.1338 p.u. Bus 18 has the lowest voltage magnitude at 0.9038 p.u.

TABLE I
Six Benchmarking Functions and Parameter Settings

Name	Functions	Value range	Minimum value
Sphere	$f_1(x) = \sum_{i=0}^{D} x_i^2$	[-100, 100]	0
Step	$f_2(x) = \sum_{i=0}^{D} (x_i + 0.5)^2$	[-100, 100]	0
Schwefel	$f_3(x) = \sum_{i=1}^{D} \lvert x_i \rvert + \prod_{i=1}^{D} \lvert x_i \rvert$	[-10, 10]	0
Ackley	$f_4(x) = -20 \cdot e^{-0.2 \cdot \sqrt{D^{-1} \cdot \sum_{i=1}^{D} x_i^2}} - e^{D^{-1} \cdot \sum_{i=1}^{D} \cos 2\pi \cdot x_i} + 20 + e$	[-32, 32]	0
Griewank	$f_5(x) = \sum_{i=1}^{D} x_i^2 / 4000 - \prod_{i=1}^{D} \cos(x_i / \sqrt{i}) + 1$	[-600, 600]	0
Rastrigin	$f_6(x) = \sum_{i=1}^{D} [x_i^2 - 10\cos(2\pi x_i) + 10]$	[-5.12, 5.12]	0

TABLE II
The Fitness Values of Three Algorithms in Benchmarking Functions

Function name	PSO			NGO			INGO		
	Best	Worst	Mean	Best	Worst	Mean	Best	Worst	Mean
Sphere	1.45E+03	2.93E+03	2.04E+03	3.7E-11	8.1E-10	2.4E-10	2.8E-64	2.7E-63	1.1E-63
Step	1.18E+03	3.11E+03	1.94E+03	8.5E-07	3.7E-05	8.5E-06	3.72E-11	3.3E-10	1.09E-10
Schwefel	2.98E+01	6.26E+01	4.01E+01	6.5E-07	4.4E-06	2E-06	4.7E-33	2.6E-32	1.2E-32
Ackley	1.71E+01	2.01E+01	1.97E+01	2.4E-06	1.4E-05	5.5E-06	4.4E-15	7.99E-15	6.6E-15
Griewank	1.44E+01	2.86E+01	2.14E+01	1.15E-10	4.2E-02	1.2E-02	0.00E+00	0.00E+00	0.00E+00
Rastrigin	2.13E+02	2.97E+02	2.52E+02	3.48E+01	5.67E+01	4.71E+01	0.00E+00	0.00E+00	0.00E+00

1) Scenario I: DG with unity power factor (UPF)

In this situation, it is assumed that the DGs supply only active power to the network and that their power factors are 1.0. The locations and dimensions of DGs are optimized using INGO and NGO algorithms to minimize instantaneous active power loss. The iterative curves of active power loss obtained by the INGO and NGO algorithms are shown in Fig. 5. When different numbers of DGs are configured, the convergence speed of INGO is substantially faster than that of NGO. The convergence value of INGO is smaller, demonstrating the effectiveness of the improvement strategy proposed in this paper.

The detailed information after the optimal configuration of different numbers of DGs using the proposed INGO algorithm is shown in TABLE III. This information includes the location and capacity of DGs, power loss P_{loss} and Q_{loss}, active and reactive network loss reductions RP_{loss} and RQ_{loss}, and indicators such as minimum voltage magnitude and voltage deviation of the system. When one, two, or three DGs are installed, the active network loss is reduced by 47.4%, 58.7%, and 65.5%, respectively, while the reactive network loss is reduced by 42.9%, 58.2%, and 64.6%, respectively. The greater the number of DGs installed, the more significant the reduction in the system's power loss. In addition, installing DGs in the power system can also improve the voltage distribution of the system. The effects on the system voltage distribution after configuring 1, 2, and 3 DGs with the INGO and NGO algorithms, respectively, are shown in Fig. 7. The bus voltage magnitudes for all configuration solutions in Fig. 7 are within the allowable range set in this paper, and the voltage distribution is significantly improved. The efficacy of INGO is verified by comparing it with the best solutions of DAPSO [38], BA [39], EGOA [40], and the original NGO, as shown in TABLE IV. When 1, 2, or 3 DGs are configured in the DS, the losses obtained by INGO are lower than those of the DAPSO, BA, EGOA, and original NGO approaches; this demonstrates the apparent advantage of the INGO algorithm in resolving the ODGA problem.

2) Scenario II: DG with optimal power factor (OPF)

Most current studies only use predetermined power factors for DG configuration optimization. They neglect how power variables of different DGs affect test network performance. Automatically finding the optimal power factor of the DG helps to further improve the performance metrics of the system compared to predetermining the power factor of the DG. Notably, thanks to recent technological advancements, DGs can operate in any power factor mode when inverters are connected, as demonstrated by the current standard IEEE 1547 [26]. For this Scenario, the researched DGs can inject both active and reactive power to RDN, matching the optimal power factor of DGs.

The three control variables of DG location, capacity, and power factor are simultaneously optimized. The INGO and NGO algorithms configure one, two, and three DGs to minimize instantaneous active power loss. The system's active network loss convergence and voltage distribution are shown in Fig. 6 and Fig. 8, respectively. When more control variables are considered, INGO still converges faster than NGO, the convergence values are smaller, and the voltage distribution at each bus is more uniform, showing that the improved technique presented in this study is still effective.

TABLE V shows the simulation results in Scenario II when the INGO algorithm is used to configure different numbers of DGs at the optimal power factor. The more DGs configured, the smaller the active and reactive network loss is, and the other metrics are further improved. Compared with the simulation results in Scenario I, the system's power loss and voltage deviation are minor when configured with the same number of DG with optimal power factor, as shown in Fig. 9.

When one, two, and three DGs at optimal power factor are installed, the active network loss is reduced by 67.84%, 86.11%, and 93.96%, and the reactive network loss is decreased by 61.69%, 85.26%, and 92.6%, respectively, with voltage deviations of 0.0163, 0.0016 and 0.0006, respectively. The minimum voltage magnitude has also increased significantly, from 0.9583 p.u with one DG to 0.9916 p.u with three DGs.

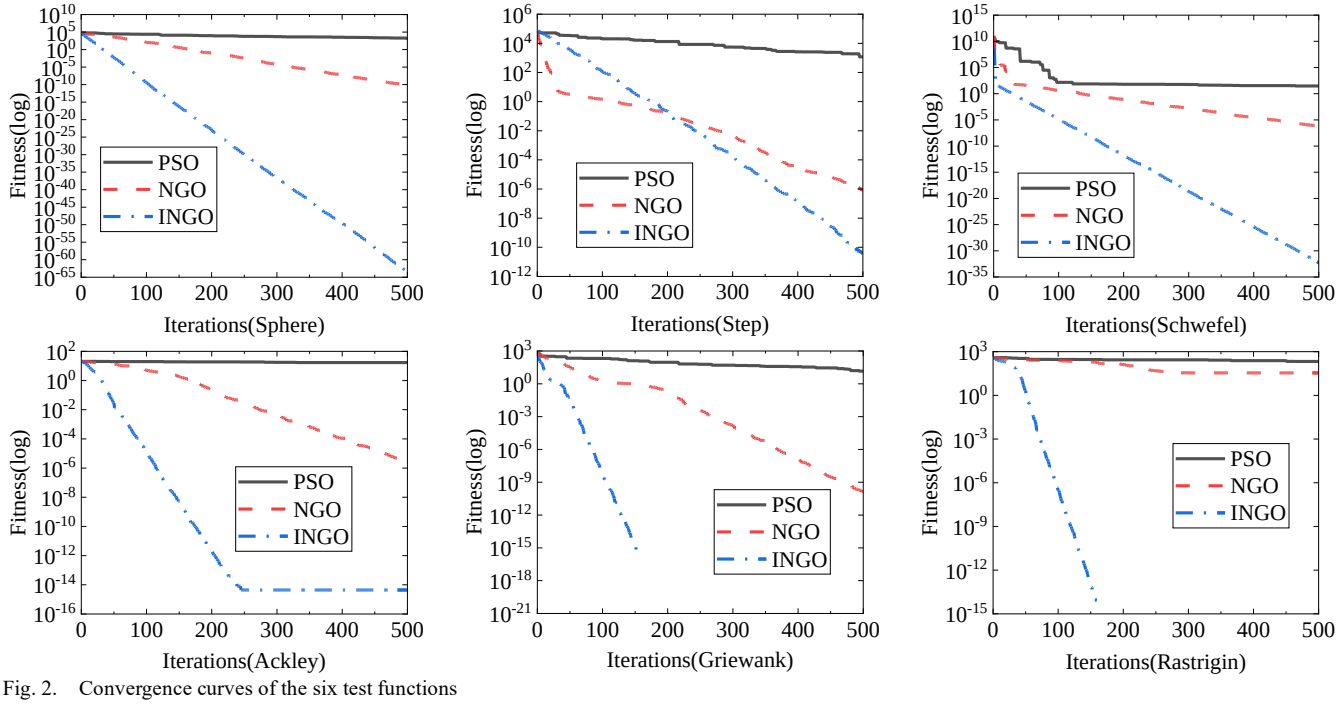

Fig. 2. Convergence curves of the six test functions

TABLE III
SIMULATION RESULTS OF INGO ALGORITHM FOR THE 33-BUS SYSTEM AT THE UNITY POWER FACTOR

	No DG	1 DG	2 DGs	3 DGs
DG size in kW (bus number)	-	2590.25(6)	851.5(13) 1157.63(30)	1053.7(30) 1091.37(24) 801.67(13)
P_{loss}(kW)	211	111.03	87.17	72.79
Q_{loss}(kVAr)	143.13	81.71	59.81	50.68
RP_{loss}(%)	-	47.4	58.7	65.5
RQ_{loss}(%)	-	42.9	58.2	64.6
V_{min}(p.u)	0.9038(18)	0.9424(18)	0.9685(33)	0.9687(33)
VD(p.u)	0.1338	0.0377	0.017	0.0151
P_{infeed}(kW)	3926	1235.78	1793.04	841.05
Q_{infeed}(kVAr)	2443.13	2381.71	2359.81	2350.68
pl(%)	-	57.47	44.9	66.1

The comparison results with previous optimization algorithms are shown in TABLE VI. The algorithm suggested in this paper (INGO) has superior performance (more active network loss reduction) than the original NGO algorithm and other algorithms published in [41-45] for all situations of 1, 2, and 3 DGs integration. The algorithm performs better when the parameters of the controlled DGs are more, indicating that the algorithm also has significant advantages in solving complex ODGA problems with more control variables or more extensive search space.

TABLE VII compares the mean and standard deviation of active power loss in the 33-bus system after 30 simulation experiments with the NGO and INGO algorithms. The INGO algorithm's mean and the standard deviation are better than the NGO algorithm's, demonstrating the effectiveness of the improved strategy.

The magnitude of power injected into the system by substation and DGs, as well as the penetration level of DGs, are illustrated in Fig. 10 after configuring different power factors and varied numbers of DGs with the INGO algorithm. When the number of DGs connected to the DS is greater, or the DGs are running at the optimal power factor, the penetration level of the DGs increases.

b: The IEEE 69-bus network

The IEEE 69-bus network from [37] is utilized to test the efficacy of the proposed approach on a medium-sized RDN. The test network consists of 69 buses and 68 branches, and the network structure is shown in Fig. 11. The network has a rated voltage of 12.66 kV, a rated capacity of 100 MVA, and the total active and reactive loads are 3.792 MW, and 2.694 MVAr, respectively. Without DG installation, the system's active and reactive power loss is 224.9 kW and 102.1 kVAr, respectively, with a voltage deviation of 0.0993 p.u. The voltage distribution of the system's buses is depicted in Fig. 14, with the maximum voltage magnitude being 1.0 p.u at bus 1 and the minimum voltage magnitude being 0.9092 p.u at bus 65.

1) Scenario I: DG with unity power factor (UPF)

To minimize active power loss, the same INGO and NGO algorithms are employed to optimize the position and capacity of 1, 2, and 3 DGs, respectively. The convergence graph and voltage distribution diagram are shown in Fig. 12 and Fig. 15, respectively. The convergence speed of INGO is still faster, and the convergence value is also smaller. The voltage distribution is more uniform and closer to 1 p.u, and the voltage magnitudes of all buses are within the range set in this paper. This indicated that the INGO algorithm is still effective in dealing with more complex ODGA problems.

TABLE VIII displays the detailed results when the INGO algorithm is used to configure 1, 2, and 3 DGs in the IEEE 69-bus test system, respectively, demonstrating a sensible configuration of DGs in the IEEE 69-bus system can significantly minimize active power loss. Similar to the results of the IEEE 33-bus system simulation, the more the number of configured DGs, the more significant the active and reactive network loss reduction, the greater the minimum voltage magnitude, and the smaller the voltage deviation. Installing one, two, or three DGs reduces active network loss by 63.01%, 64.81%, and 69.03%, respectively, and reactive network loss by 60.31%, 64.81%, and 65.67%. The minimum voltage is raised from 0.9092 to 0.9683, 09789, and 0.979, while the voltage deviation is lowered from 0.0993 to 0.02, 0.006, and 0.0053, respectively.

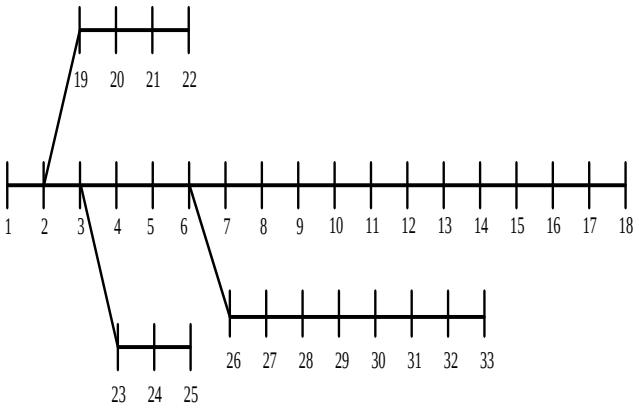

Fig. 3. Structure diagram of the 33-bus test system

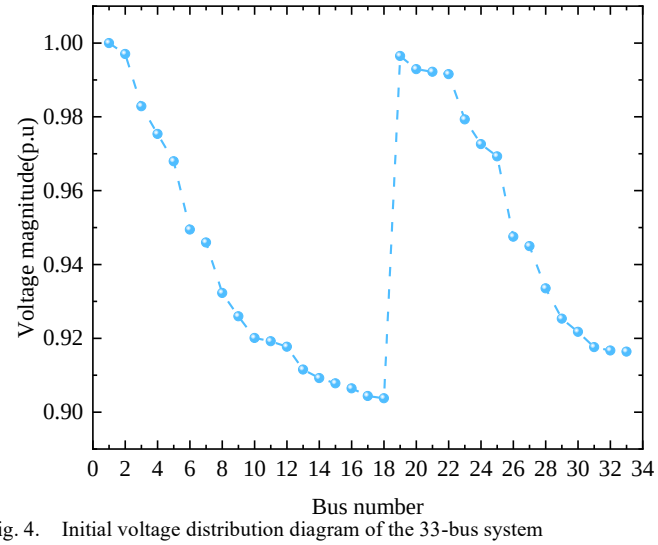

Fig. 4. Initial voltage distribution diagram of the 33-bus system

TABLE IV
COMPARISON OF THE RESULTS OF THE INGO ALGORITHM WITH OTHER ALGORITHMS FOR THE 33-BUS SYSTEM AT THE UNITY POWER FACTOR

Scenario	Algorithm	DG size in kW(bus number)			P_{loss}(kW)	RP_{loss}(%)
		DG1	DG2	DG3		
No DG	-	-	-	-	211	-
1 DG	INGO	2590.25(6)	-	-	111.03	47.38
	NGO	1695.98(7)	-	-	120.98	42.66
	DAPSO[38]	1212(8)	-	-	127.17	39.73
	BA[39]	816.3(15)	-	-	137.2	34.98
	EGOA[40]	902.9(17)	-	-	141.12	33.12
2 DGs	INGO	851.5(13)	1157.63(30)	-	87.17	58.69
	NGO	1351.23(28)	804.53(13)	-	89.04	57.8
	DAPSO[38]	1227(13)	738(32)	-	95.93	54.54
	BA[39]	952.4(15)	952.4(25)	-	112.88	46.5
	EGOA[40]	962.3(17)	184.5(18)	-	128.56	39.07
3 DGs	INGO	1053.7(30)	1091.37(24)	801.67(13)	72.79	65.5
	NGO	995.29(30)	814.62(13)	1258.84(3)	78.63	62.73
	DAPSO[38]	681(10)	600(18)	719(31)	92.55	56.14
	BA[39]	816.3(15)	952.35(25)	952.35(30)	75.05	64.43
	EGOA[40]	674.81(17)	171.04(18)	1032.31(31)	87.31	58.62

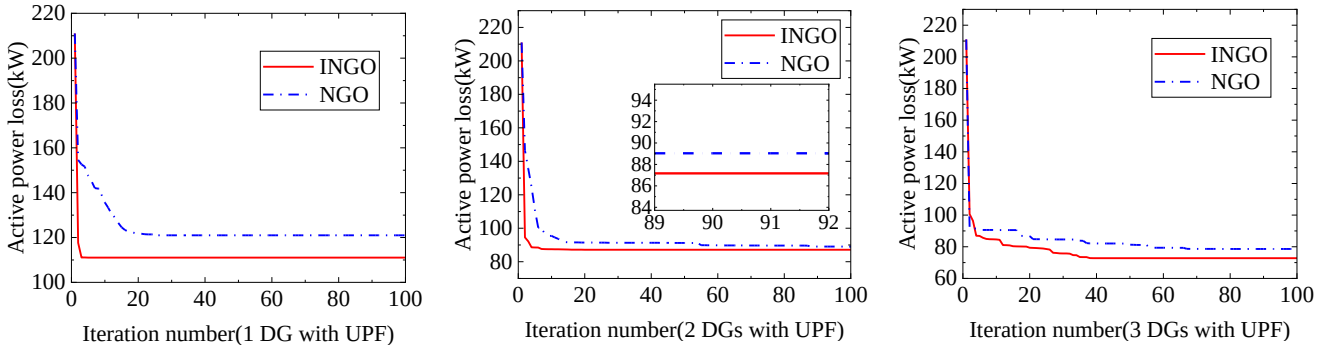

Fig. 5. INGO and NGO convergence curves of the 33-bus system at the unity power factor

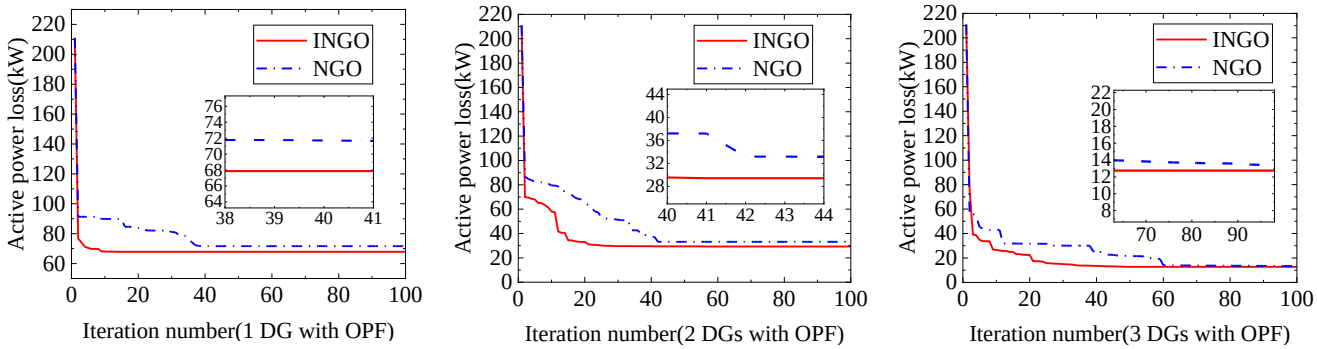

Fig. 6. INGO and NGO convergence curves of the 33-bus system at the optimal power factor

TABLE V
SIMULATION RESULTS OF INGO ALGORITHM FOR THE 33-BUS SYSTEM AT THE OPTIMAL POWER FACTOR

	No DG	1 DG	2 DGs	3 DGs
DG size in kW/*pf* (bus number)	-	2558.51/0.82368(6)	1240.43/0.8(30) 819.03/0.883437(13)	1048.85/0.883901(24) 739.22/0.882599(14) 1156.55/0.8(30)
P_{loss}(kW)	211	67.87	29.31	12.74
Q_{loss}(kVAr)	143.13	54.84	29.1	10.58
RP_{loss}(%)	-	67.84	86.11	93.96
RQ_{loss}(%)	-	61.69	85.26	92.6
$V_{\min}$(p.u)	0.9038(18)	0.9583(18)	0.9804(25)	0.9916(8)
VD(p.u)	0.1338	0.0163	0.0016	0.0006
P_{infeed}(kW)	3926	1224.36	1684.85	783.12
Q_{infeed}(kVAr)	2443.13	593.46	964.39	494.47
pl(%)	-	69.71	56.03	78.88

The comparison of the simulation results of the INGO algorithm with those of IA [43], CF-PSO [46], EA [47], AM-PSO [25], TLBO [48], and the original NGO algorithm is shown in TABLE IX. When configured with the same number of DGs, the active network loss of the INGO method suggested in this paper is lower than the active network loss of previous algorithms.

2) Scenario II: DG with optimal power factor (OPF)

When the power factor of DG is not predetermined, the INGO and NGO algorithms are used to optimize DG's location, capacity, and power factor simultaneously. The active power loss iteration curve is shown in Fig. 13. In the

medium-sized test network, increasing the dimensionality of the control variables, the INGO effect still outperforms the NGO algorithm, with faster convergence and lower active network loss. The impact of configuring different numbers of DGs using the INGO and NGO algorithms on system voltage distribution is demonstrated in Fig. 16. Although some buses have voltage magnitudes greater than 1 p.u, they are all within the range allowed in this paper. In this scenario, with the same number of DGs configured, the voltage distribution of INGO is still more uniform than NGO's. The more the number of DGs configured, the closer the voltage magnitude of each bus is to the reference voltage magnitude.

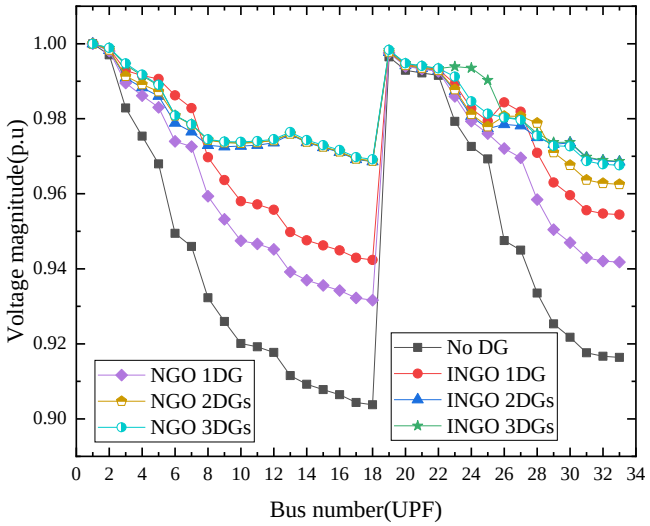

Fig. 7. Voltage distribution in the 33-bus system for different cases at the unity power factor

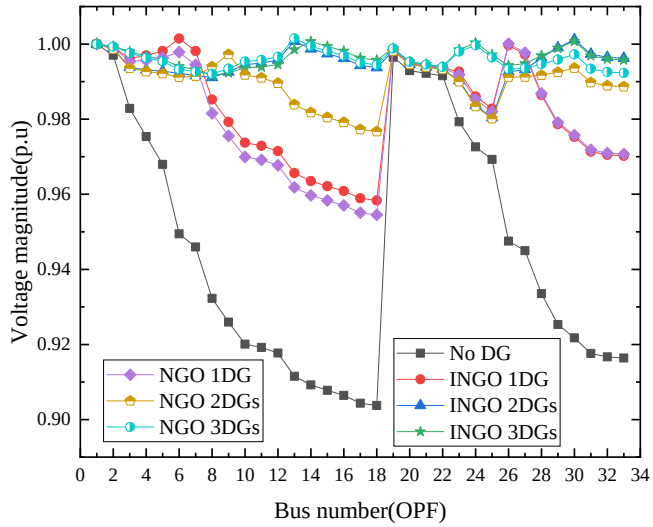

Fig. 8. Voltage distribution in the 33-bus system for different cases at the optimal power factor

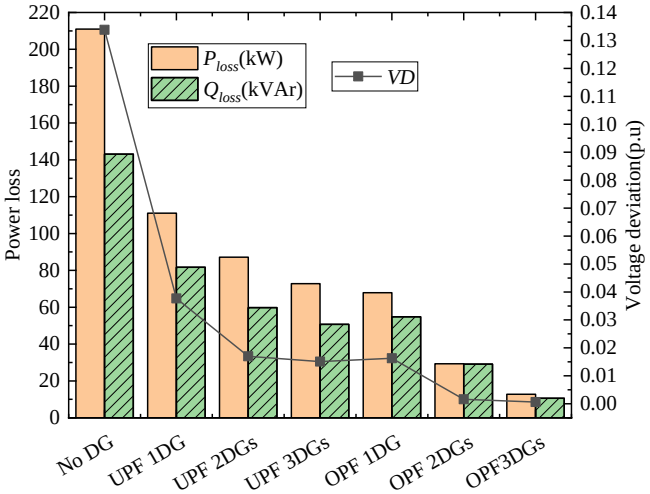

Fig. 9. Power loss and voltage deviation in the 33-bus system after configuring different DGs using the INGO algorithm

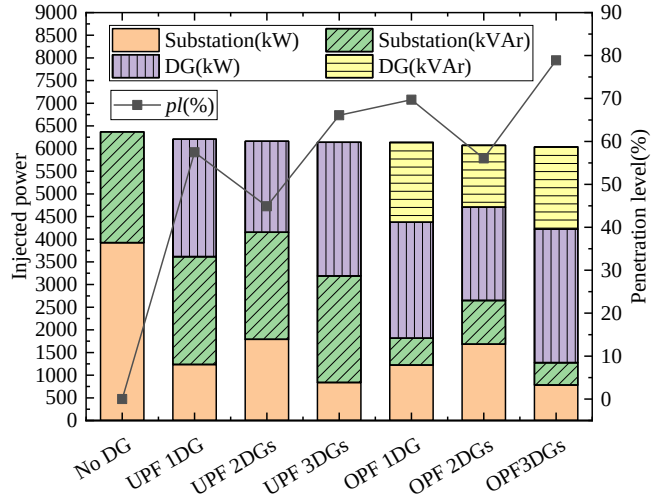

Fig. 10. Power injected and DGs' penetration level after configuration of different DGs using INGO algorithm in the 33-bus system

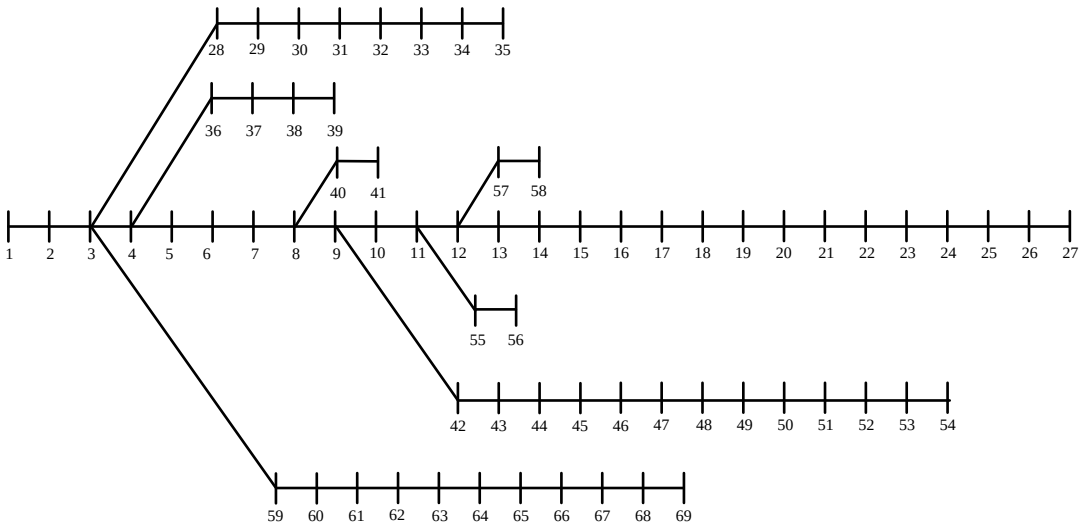

Fig. 11. Structure diagram of the 69-bus test system

TABLE VI
COMPARISON OF THE RESULTS OF THE INGO ALGORITHM WITH OTHER ALGORITHMS FOR THE 33-BUS SYSTEM AT THE OPTIMAL POWER FACTOR

Scenario	Algorithm	DG size in kW/power factor(bus number)			P_{loss}(kW)	RP_{loss}(%)
		DG1	DG2	DG3		
No DG	-	-	-	-	211	-
1 DG	INGO	2558.51/0.8237(6)	-	-	67.87	67.84
	NGO	2581.2/0.8291(26)	-	-	71.65	66.04
	Analytical[41]	2215/0.8907(6)	-	-	69.01	67.29
	EPF[41]	2213/0.8907(6)	-	-	69	67.3
	HPSO[42]	1485.5/0.85(14)	-	-	112.8	46.54
2 DGs	INGO	1240.43/0.8(30)	819.03/0.8834(13)	-	29.31	86.11
	NGO	985.83/0.8521(9)	1009.91/0.8037(30)	-	33.16	84.28
	Analytical[41]	2215/0.8907(6)	1072/0.8907(28)	-	55.85	73.53
	EPF[41]	2213/0.8907(6)	1069/0 .8907(28)	-	55.73	73.59
	HPSO[42]	742.8/0.85(17)	742.8/0.85(31)	-	52.72	75.01
3 DGs	INGO	1048.85/0.8839(24)	739.22/0.8826(14)	1156.55/0.8(30)	12.74	93.96
	NGO	1061.19/0.8(30)	809.19/0.8806(13)	943.53/0.8252(24)	13.31	93.69
	IA[43]	900.4/0.82(6)	629.8/0.82(14)	900.4/0.82(30)	22.29	89.44
	HHO[44]	913.05/0.85(12)	882.86/0.82(24)	1079.05/0.83(30)	14.94	92.92
	QODELFA[45]	758.28/0.866(13)	1027.3/0.866(24)	1213.9/0.866(30)	15.35	92.73

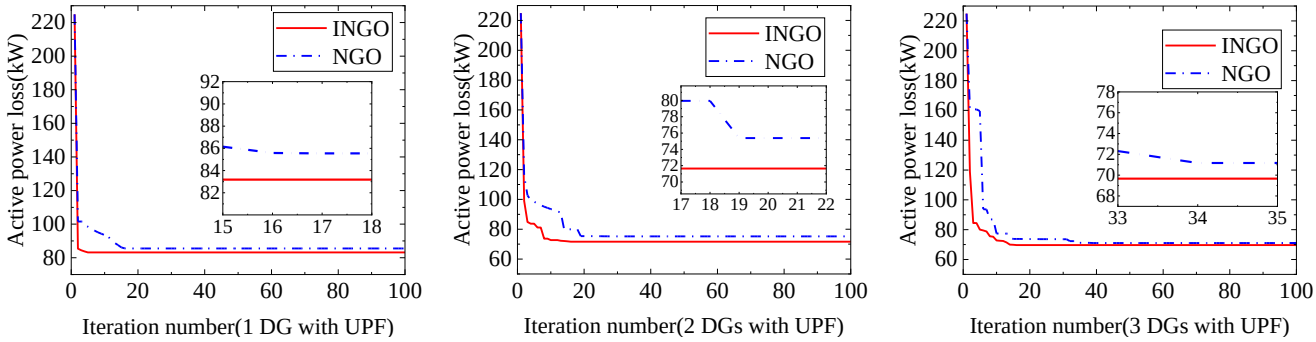

Fig. 12. INGO and NGO convergence curves of the 69-bus system at the unity power factor

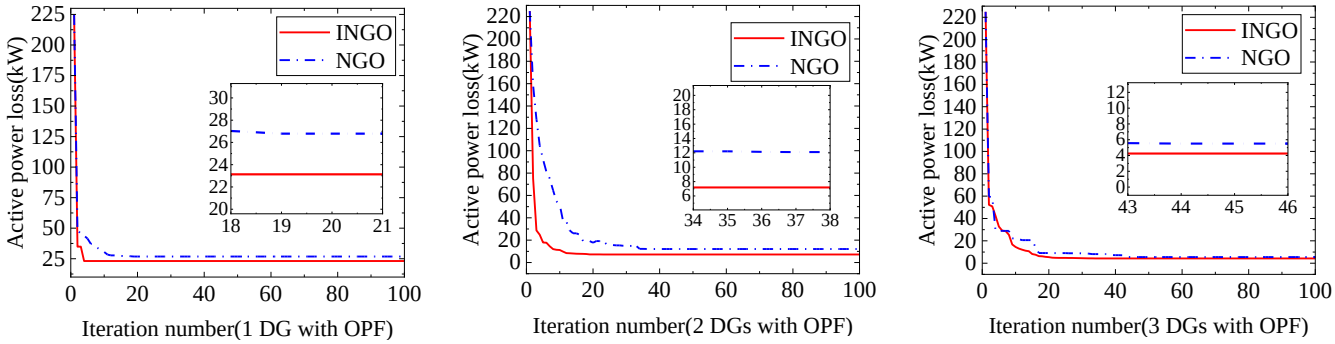

Fig. 13. INGO and NGO convergence curves of the 69-bus system at the optimal power factor

TABLE VII
THE AVERAGE VALUE AND STANDARD DEVIATION OF THE P_{LOSS}(KW) IN 33-BUS SYSTEM

case		NGO		INGO	
		Mean(kW)	Std	Mean(kW)	Std
UPF	1DG	122.89	0.712475	111.15	0.265411
	2DGs	90.27	0.923601	87.45	0.285795
	3DGs	79.24	0.697652	73.17	0.454712
OPF	1DG	72.01	0.804441	68.46	0.324112
	2DGs	34.26	0.726104	29.51	0.309415
	3DGs	14.52	0.891207	12.9	0.202265

After configuring different DG numbers with the INGO algorithm, the detailed information is shown in TABLE X. Fig. 17 compares the power loss and voltage deviation in Scenarios I and II. Similar to the simulation results of the 33-bus system, when the configured DGs emit both active and reactive power, the power loss of the system is reduced substantially, and the more the number of installed DGs, the smaller the loss. When 1, 2, and 3 DGs are installed at optimal power factor, the active network loss of the system is much less than the power loss incurred by installing the same number of DGs in Scenario I. The minimum voltage magnitudes and the voltage deviations are also substantial improvements compared to the data in Scenario I.

TABLE XI compares the simulation results of the INGO algorithm's optimal configuration with those of other algorithms to validate its effectiveness in handling the high-dimensional ODGA problem in medium-sized test networks. The results of the INGO algorithm outperform the results of the IA [43], CF-PSO [46], HCF [49], EPF [41], and EA [47] algorithms in terms of active power loss reduction. In contrast, the performance of the original NGO algorithm is slightly inferior to that of the other compared algorithms, once again demonstrating the effectiveness of the improved strategy proposed in this paper.

The magnitude of power injected into the system by substation and DGs and the penetration level of DGs are illustrated in Fig. 18 after configuring different power

factors and DG amounts using the INGO algorithm. The lower the total power pumped into the system by the substation and DGs, the higher the DG penetration level.

B. *Case study 2: Varied load and generation*

a: System load curve

The hourly load variation considered in this study is shown in Fig. 19, where the vertical coordinate indicates the value of the load at that moment as a percentage of the peak load. This data is obtained by averaging the seasonal load variation curves described in [50].

b: Variation of DG generation

Since hourly changes in sunlight intensity and wind speed will lead to changes in DG generation, the hourly output variation of PV and WT considered in this study is shown in Fig. 20, where the vertical coordinates indicate the actual generation of the generator at the current moment (normalized). The curve is plotted by averaging the seasonal output variation curves of both PV and WT described in [50].

c: The IEEE 33-bus network

The daily active and reactive energy losses without DG installations are 1827.42 kWh and 1238.33 kVArh, respectively, based on the load curve depicted in Fig. 19. In contrast, the daily active and reactive energy injected from the substation is 56.02 MWh and 34.79 MVArh, respectively, with a *DVD* of 1.154.

In this case, the locations, capacities, and power factors of three different types of DGs, including PVs, WTs, and CGs, are optimized simultaneously to minimize DEL_P, considering the generation variation of DGs and the load variation of the system. Assuming that the output of CG remains constant throughout the day, the normalized daily output power of PV and WT is shown in Fig. 20.

The best choice for configuring the three types of DGs (including CGs, PVs, and WTs) with the INGO algorithm to reduce DEL_P is shown in TABLE XII. Both UPF and OPF cases are considered in the installation of all DGs. TABLE XIII compares the effects of the best options for allocating CGs, PVs, and WTs on the DS. The daily energy loss reduction of DS for all cases is shown in Fig. 21.

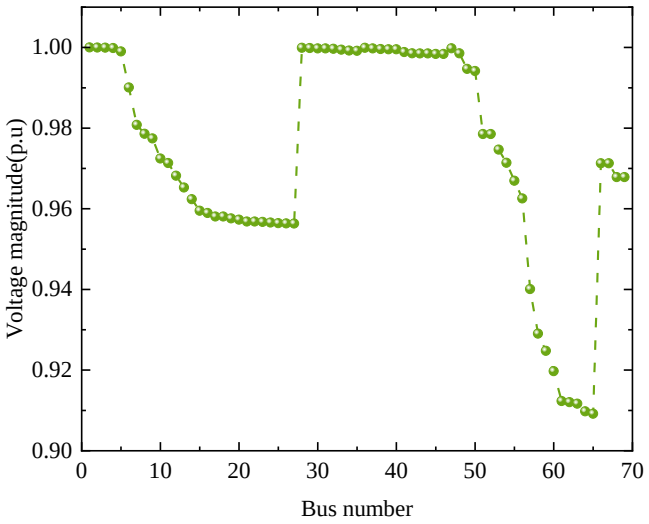

Fig. 14. Initial voltage distribution diagram of the 69-bus system

TABLE VIII
SIMULATION RESULTS OF INGO ALGORITHM FOR THE 69-BUS SYSTEM AT THE UNITY POWER FACTOR

	No DG	1 DG	2 DGs	3 DGs
DG size in kW (bus number)	-	1872.65(61)	531.17(17) 1781.47(61)	459.69(66) 1726.93(61) 399.28(18)
P_{loss}(kW)	224.9	83.18	71.65	69.66
Q_{loss}(kVAr)	102.1	40.52	35.93	35.05
RP_{loss}(%)	-	63.01	68.14	69.03
RQ_{loss}(%)	-	60.31	64.81	65.67
V_{min}(p.u)	0.9092(65)	0.9683(27)	0.9789(65)	0.979(65)
VD(p.u)	0.0993	0.02	0.006	0.0053
P_{infeed}(kW)	4016.9	2002.53	1551.01	1275.76
Q_{infeed}(kVAr)	2796.1	2734.52	2729.93	2729.05
pl(%)	-	39.48	48.88	54.69

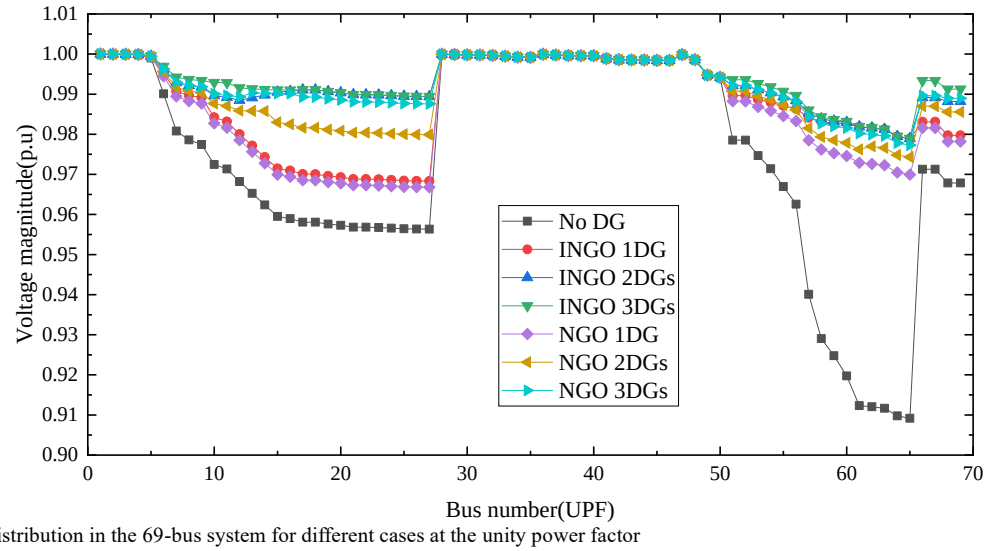

Fig. 15. Voltage distribution in the 69-bus system for different cases at the unity power factor

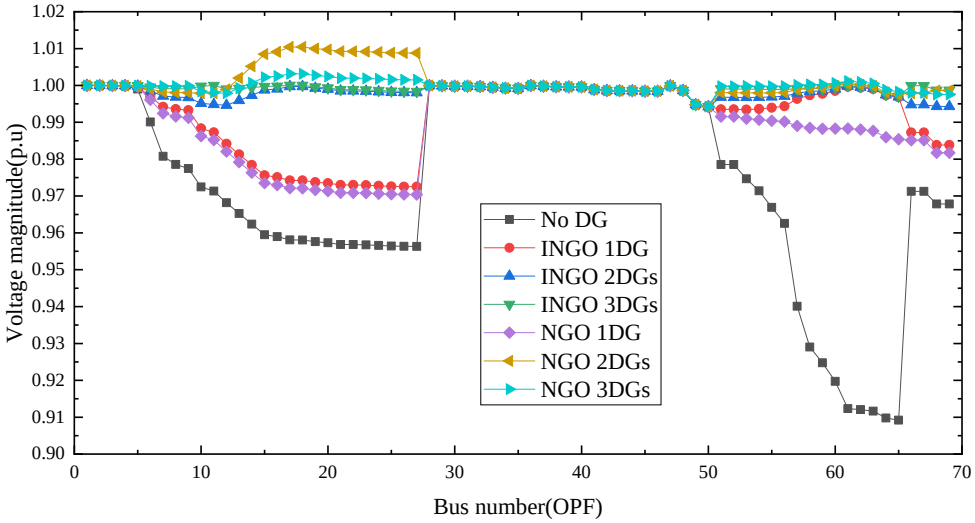

Fig. 16. Voltage distribution in the 69-bus system for different cases at the optimal power factor

TABLE IX
COMPARISON OF THE RESULTS OF THE INGO ALGORITHM WITH OTHER ALGORITHMS FOR THE 69-BUS SYSTEM AT THE UNITY POWER FACTOR

Scenario	Algorithm	DG size in kW(bus nuber)			P_{loss}(kW)	RP_{loss}(%)
		DG1	DG2	DG3		
No DG	-	-	-	-	224.9	-
1 DG	INGO	1872.65(61)	-	-	83.18	63.015
	NGO	1614.85(61)	-	-	85.54	61.965
	IA[43]	1900(61)	-	-	83.24	62.992
	CF-PSO[46]	1806.2(61)	-	-	83.37	62.93
	EA[47]	1878(61)	-	-	83.23	62.987
2 DGs	INGO	531.17(17)	1781.47(61)	-	71.65	68.141
	NGO	426.13(14)	1637.99(62)	-	75.2	66.563
	IA[43]	510(17)	1700(61)	-	71.95	68.008
	CF-PSO[46]	511(17)	1806.2(61)	-	71.71	68.115
	AM-PSO[25]	520(17)	1720(61)	-	71.8	68.075
3 DGs	INGO	459.69(66)	1726.93(61)	399.28(18)	69.66	69.026
	NGO	1722.06(61)	407.38(16)	192.02(13)	71.02	68.422
	IA[43]	1700(61)	510(17)	340(11)	69.96	68.893
	CF-PSO[46]	1806.2(61)	511(17)	719(50)	70.19	68.791
	TLBO[48]	1160.1(62)	990.1(61)	1013.4(13)	82.17	63.464

TABLE X
SIMULATION RESULTS OF INGO ALGORITHM FOR THE 69-BUS SYSTEM AT THE OPTIMAL POWER FACTOR

	No DG	1 DG	2 DGs	3 DGs
DG size in kW/*pf* (bus number)	-	1828.41/0.8149(61)	1734.68/0.8139(61) 522.04/0.8283(17)	1672.89/0.8138(61) 380.1/0.8346(18) 501.69/0.8145(11)
P_{loss}(kW)	224.9	23.14	7.19	4.26
Q_{loss}(kVAr)	102.1	14.36	8.04	6.75
RP_{loss}(%)	-	89.71	96.8	98.11
RQ_{loss}(%)	-	85.94	92.13	93.39
$V_{\min}$(p.u)	0.9092(65)	0.9725(27)	0.99426(50)	0.99427(50)
VD(p.u)	0.0993	0.0118	0.0004	0.0001
P_{infeed}(kW)	4016.9	1986.73	1542.47	1241.58
Q_{infeed}(kVAr)	2796.1	1407.85	1110.48	897.72
pl(%)	-	47.96	59.23	67.12

The reasonable allocation of all three DG types in the system can lower the daily energy loss. The more DGs installed, the smaller the daily active and reactive energy loss. When three CGs, PVs, and WTs are configured, and all three DGs are at unity power factor, the DEL_P is decreased by 62.34%, 35.19%, and 60.62%, respectively, from 1827.42 kWh to 688.14 kWh, 1184.44 kWh, and 719.67 kWh. The DEL_P after installing PV is the greatest compared to the other two types of generators. The DEL_P after installing WTs is slightly higher than the DEL_P after installing CGs, and both are significantly reduced. When the power factor of all three generators is optimal, the daily energy loss is further reduced. When three CGs, PVs, and WTs are installed, the DEL_P drops to 166.58kWh, 891.29kWh, and 214.44kWh, respectively. The reduction is 90.88%, 51.23%, and 88.27%, respectively, and the energy loss of CGs and WTs is still much less than that of PVs. Because PVs are not generating electricity for 11 hours out of 24 hours a day, while CGs and WTs generate electricity every hour. The difference between the CGs and WTs is that the energy generated by the former is fixed each hour, while the latter is variable each hour. Although the CG is better than the WT, the DEL_P difference is insignificant. WTs outperform PVs when REDGs replace CGs and reduce DEL_P.

Fig. 22 demonstrates the hourly active power loss over a

day for DGs configured with various amounts, power factors, and types. Due to high light intensity from 8:00 to 16:00, PV installation outperformed WT. The CG has the lowest energy loss practically all hours. However, the total energy loss after installing CGs is about the same as WTs, and the hourly energy loss curves almost overlap.

Fig. 23 shows the voltage deviation for each hour of the day for different configuration scenarios. The voltage deviation of CGs is lower than that of WTs in all periods, and the higher the number of CGs, the lower the voltage deviation. For both WTs and PVs, PVs are the best and even better than CGs from 8:00 to 16:00, but the total voltage deviation is lower for WTs.

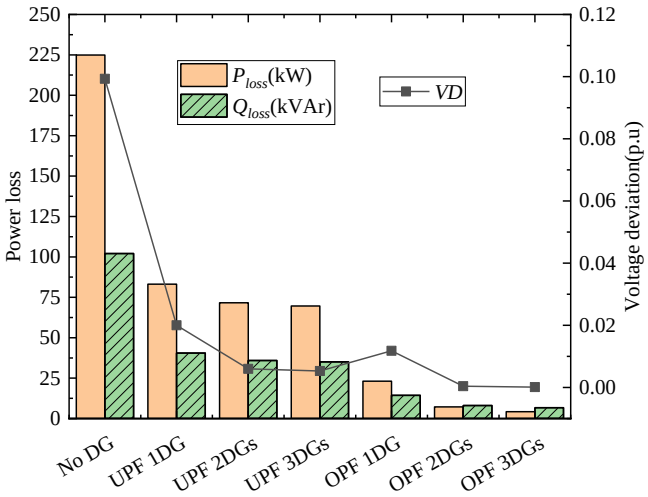

Fig. 17. Power loss and voltage deviation in the 69-bus system after configuring different DGs using the INGO algorithm

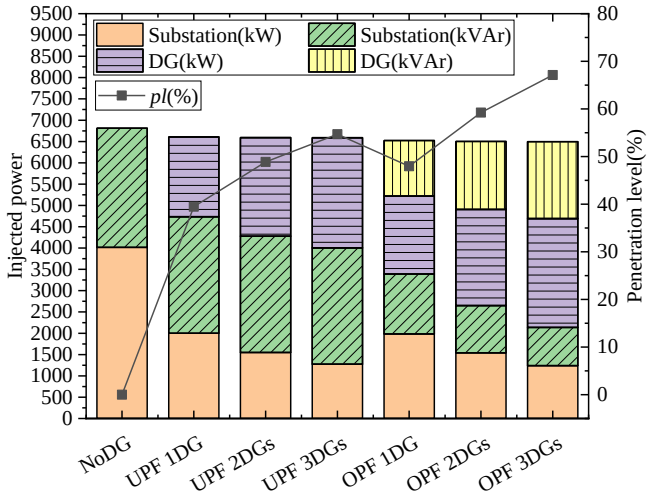

Fig. 18. Injected power and DGs' penetration levels after configuration of different DGs using INGO algorithm in the 69-bus system

TABLE XI
COMPARISON OF THE RESULTS OF THE INGO ALGORITHM WITH OTHER ALGORITHMS FOR THE 69-BUS SYSTEM AT THE OPTIMAL POWER FACTOR

Scenario	Algorithm	DG size in kW/power factor(bus number)			P_{loss}(kW)	RP_{loss}(%)
		DG1	DG2	DG3		
No DG	-	-	-	-	224.9	-
1 DG	INGO	1828.41/0.8149(61)	-	-	23.14	89.71
	NGO	1584.59/0.8256(61)	-	-	26.79	88.088
	IA[43]	2243/0.82(61)	-	-	23.18	89.693
	CF-PSO[46]	2207/0.8241(61)	-	-	23.26	89.658
	HCF[49]	2300/0.85(61)	-	-	23.98	89.337
2 DGs	INGO	1734.68/0.8139(61)	522.04/0.8283(17)	-	7.19	96.803
	NGO	1802.8/0.8739(61)	787.01/0.8888(18)	-	12.1	94.62
	IA[43]	2195/0.82(61)	659/0.82(17)	-	7.41	96.705
	CF-PSO[46]	2107.5/0.8272(61)	641.6/0.8161(17)	-	7.31	96.75
	EPF[41]	1571/0.82(61)	775/0.82(49)	-	21.63	90.382
3 DGs	INGO	1672.89/0.8138(61)	380.1/0.8346(18)	501.69/0.8145(11)	4.26	98.106
	NGO	530.29/0.8293(17)	1694.55/0.8209(61)	452.1/0.8348(9)	5.52	97.546
	IA[43]	2073/0.82(61)	622/0.82(17)	829/0.82(50)	5.07	97.746
	CF-PSO[46]	2086/0.8318(61)	613.4/0.8279(18)	845.4/0.8276(50)	5.17	97.701
	EA[47]	548/0.82(11)	380/0.83(18)	1733/0.82(61)	4.48	98.008

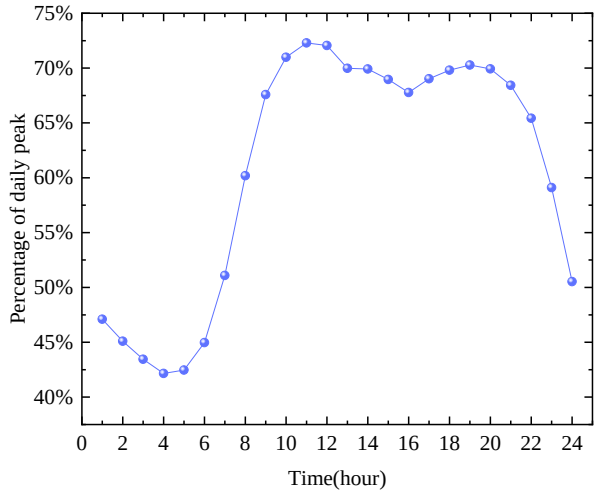

Fig. 19. Hourly load curve

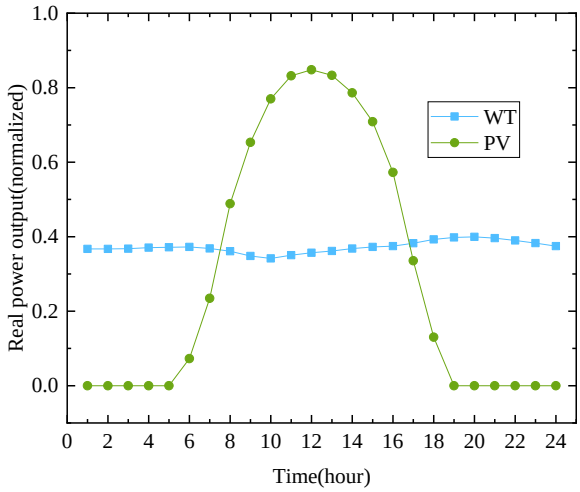

Fig. 20. Hourly output curves of PV and WT

TABLE XII
OPTIMAL CONFIGURATION SCHEME FOR DGS IN 33-BUS SYSTEM (INCLUDING CGS, PVS, AND WTS)

		CG		PV		WT	
		DG size in kW (bus number)	*pf*	DG size in kW (bus number)	*pf*	DG size in kW (bus number)	*pf*
1 DG	UPF	1542.45(6)	1	2537.25(6)	1	3677.85(6)	1
	OPF	1531.79(6)	0.824	2522.08(6)	0.8239	3677.85(26)	0.8502
2 DGs	UPF	698.71(30)	1	848.12(13)	1	1874.26(30)	1
		516.3(13)	1	1147.63(30)	1	1384.95(13)	1
	OPF	497.84(13)	0.8838	820.04(13)	0.8836	1335.5(13)	0.8838
		753.93(30)	0.8	1240.91(30)	0.8	2022.47(30)	0.8
3 DGs	UPF	642.81(30)	1	798.58(13)	1	1183.9(14)	1
		661.23(24)	1	1044(30)	1	941.63(25)	1
		468.11(14)	1	1079.56(24)	1	1552.21(30)	1
	OPF	637.08(24)	0.884	1158.08(30)	0.8	850.6(25)	0.9048
		703.79(30)	0.8	1044.4(24)	0.884	1702.73(30)	0.8
		450.07(14)	0.8829	741.13(14)	0.8827	1124.44(14)	0.8824

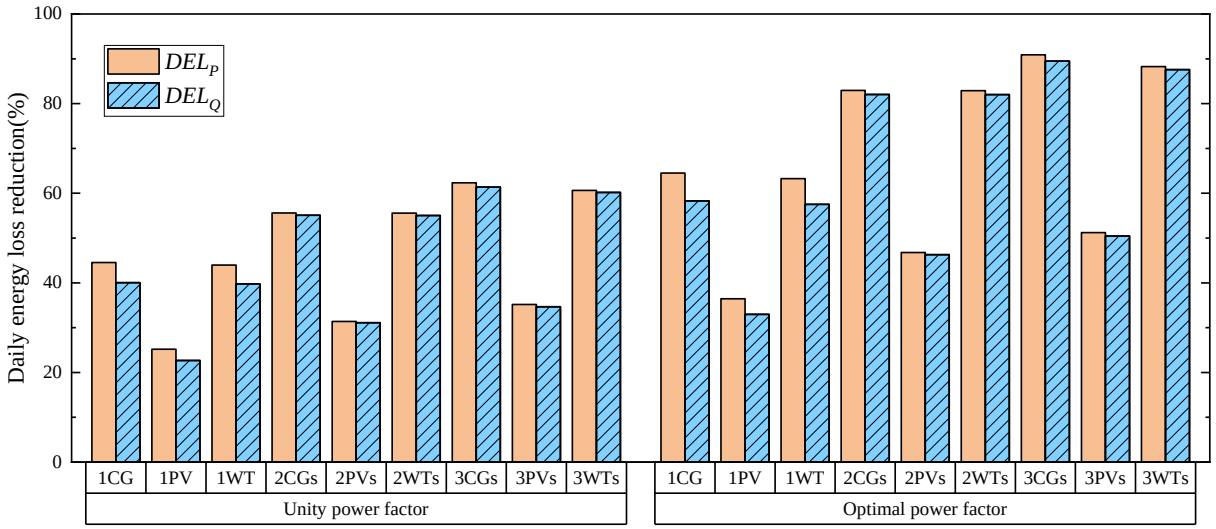

Fig. 21. Percentage reduction in daily energy loss for all configuration cases in the 33-bus system

Fig. 24 depicts the substation's and DG's relative injected energy and penetration levels. The greater the number of DGs installed, the lesser the sum of energy injected by the substation and DGs. Under the same conditions, the total energy injected by the substation and DGs following the installation of CGs in the DS is the least, and the DG penetration levels are the highest. On the contrary, the total energy input after installing PVs is the highest, while DG penetration is the lowest. The distinctions between CGs and WTs are minor. When operating at the optimal power factor, the total energy injected by the substation and DGs is reduced further, and the penetration level of DGs is increased. The installation of WTs is also preferable to PVs to reduce the total energy injection into the system and increase the DG's penetration level.

d: The IEEE 69-bus network

In this study, to verify the effectiveness of the proposed optimization framework in solving the dynamic OADG problem in a more extensive test system, we also configured different numbers of CGs, PVs, and WTs in the 69-bus RDN. The same load profile and generator output curve as in the 33-bus RDN were used to minimize the system's active power loss throughout the day. Without the installation of DGs, the DEL_P of the system is 1936.65 kWh, and the DEL_Q is 882.55 kVArh. The active energy injected into the system by the substation is 57.247 MWh, and the reactive energy is 40.183 MVArh.

TABLE XIV shows the optimal solutions for configuring three different types of DGs (CGs, PVs, and WTs) using the INGO algorithm, where the UPF and OPF are considered for all DGs. TABLE XV displays the system performance indicators following the configuration of three different DGs, including energy loss, voltage deviation, energy injection, and penetration level. Fig. 25 shows the percentage reduction in all-day energy loss under different setup scenarios. Fig. 25 and TABLE XV demonstrate that energy loss is reduced after using the INGO method to configure three distinct DG types in the 69-bus test system. Among them, configuring CGs has the best effect, configuring WTs has a slightly poorer effect than configuring CGs, and configuring PVs has the most impoverished effect. After taking into account the influence of the OPF, the system's energy loss reduction is further increased, and the more DGs that are installed, the better the result. When three CGs, PVs, and WTs are configured with optimal power factors, active energy loss is decreased by 1842.75kWh, 1038.77kWh, and 1834.83kWh, by 95.15%, 53.64%, and 94.74%. The active energy loss is only decreased by 59.49%, 33.64%, and 59.44% when only one DG with a unity power factor is specified.

Fig. 26 and Fig. 27 represent the active power loss and voltage deviation in the 69-bus test system at various times of the day after configuring different numbers, different power factors, and different types of DGs. According to Fig. 26, although the power loss is lowest most of the time after the installation of CGs, the difference with the loss after the building of WTs is relatively tiny. When only 1 or 2 DGs are installed, the loss curves of CGs and WTs almost coincide, and only at certain moments is the value of CGs slightly

lower than that of WTs. As seen in Fig. 27, the total voltage deviation after the installation of CGs is also the smallest but not much different from that after WTs installation. In addition, from the three graphs, we also found that although the overall effect is worse after the installation of PVs, in the period of eight in the morning to four in the afternoon, the installation of PVs is not weaker than the other two DGs, or even better performance. During these hours, the active power losses of the system with PVs installation were lower than those with WTs installation, and the voltage deviation with PVs installation was lower than those with the other two DGs.

Fig. 28 depicts the DG, substation energy injection, and DG penetration level for all configuration cases in the 69-bus test system. According to Fig. 28, the bigger the number of installations for the same type of DGs, the lower the total energy injected into the system by DGs and substations, and the higher the penetration level of DGs. For different types of DGs, when the number of installations is the same, the penetration level after installing CGs is the highest, and the penetration level after installing PVs is the lowest.

When the effect of the optimal power factor is added, the penetration level of the DG is further increased. When three CGs with optimal power factor were installed, the penetration level of the CGs reached 67.14%. In contrast, when the power factor was 1, the penetration level of three CGs was only 46.59%.

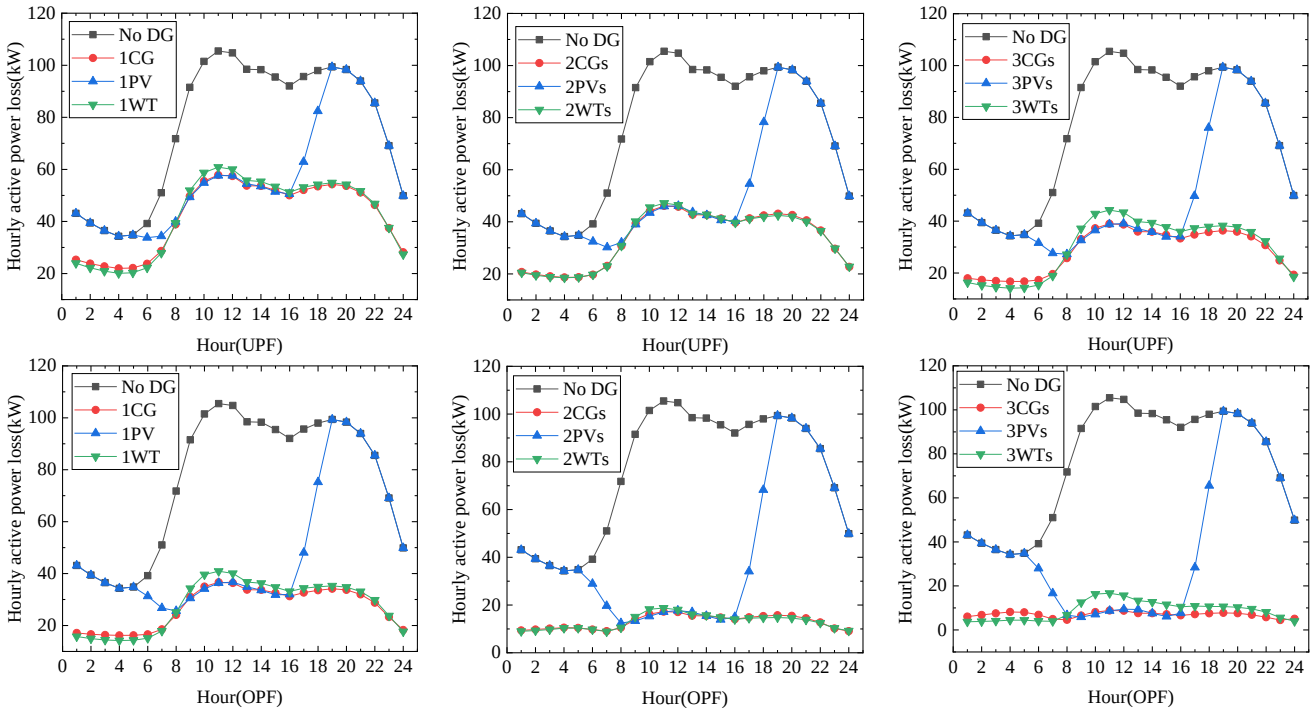

Fig. 22. Comparison of hourly active power loss in all configuration cases in the 33-bus system

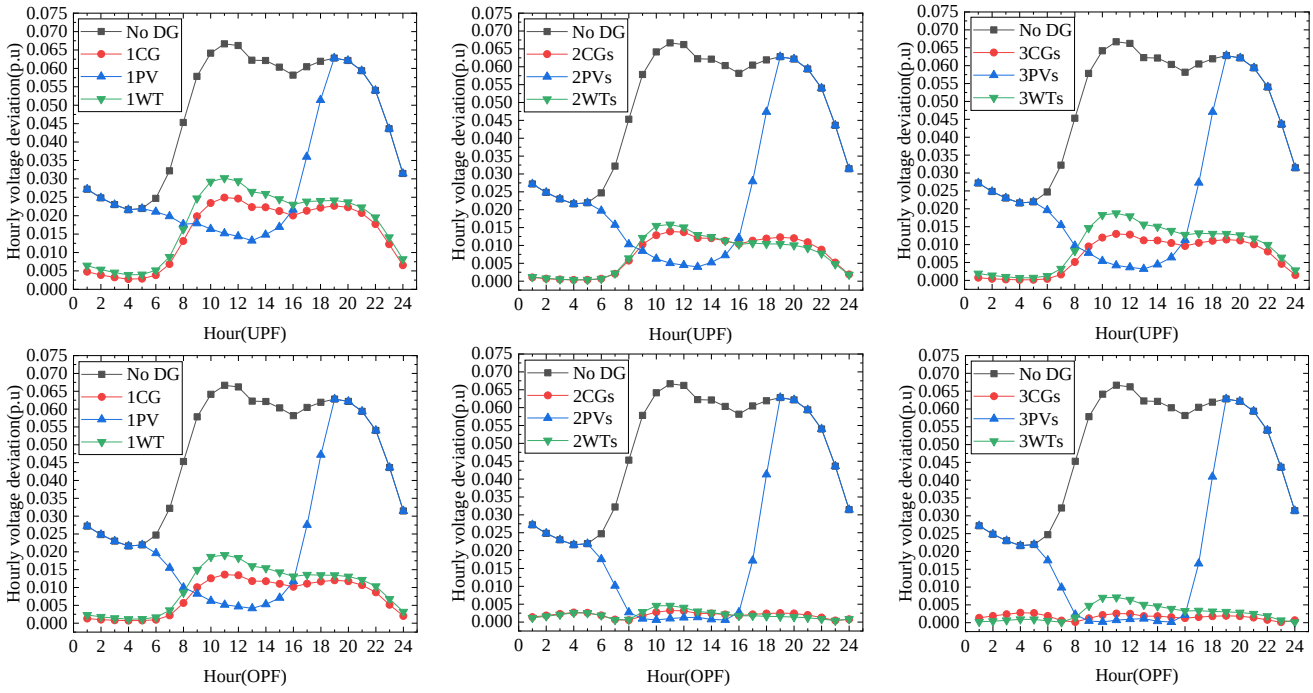

Fig. 23. Comparison of hourly voltage deviation in all configuration cases in the 33-bus system

TABLE XIII
IMPACT OF THE OPTIMAL CONFIGURATION OF DIFFERENT DGS ON THE 33-BUS SYSTEM

DG number	*pf*	Energy loss		*DVD*	Energy from DG			Energy from Substation		
		kWh	kVArh		MWh	MVArh	*pl*(%)	MWh	MVArh	*pl*(%)
No DG	-	1827.42	1238.33	1.154	-	-	-	56.02	34.79	100
1 CG	UPF	1013.67	742.41	0.366	37.02	-	48.82	18.18	34.29	51.18
	OPF	648.49	516.36	0.181	36.76	25.28	68.95	18.07	8.78	31.05
2 CGs	UPF	811.37	556.25	0.182	29.16	-	40.53	25.84	34.1	59.47
	OPF	311.73	222.22	0.048	30.04	19.9	56.17	24.46	13.87	43.83
3 CGs	UPF	688.14	478.21	0.167	42.53	-	54.02	12.35	34.03	45.98
	OPF	166.58	130.11	0.039	42.98	26.5	78.96	11.37	7.18	21.04
1 PV	UPF	1367.1	957.45	0.708	18.43	-	26.67	37.12	34.51	73.33
	OPF	1161.23	829.97	0.604	18.32	12.6	34.1	37.03	21.78	65.9
2 PVs	UPF	1253.62	853.04	0.606	14.5	-	21.33	40.94	34.4	78.67
	OPF	972.41	665.07	0.53	14.97	9.92	27.66	40.19	24.3	72.34
3 PVs	UPF	1184.44	809.07	0.597	21.23	-	30.47	34.14	34.36	69.53
	OPF	891.29	613.53	0.525	21.39	13.19	38.77	33.69	20.97	61.23
1 WT	UPF	1023.89	745.89	0.428	32.87	-	44.54	22.34	34.29	55.46
	OPF	671.18	525.95	0.237	32.87	20.35	59.86	21.99	13.73	40.14
2 WTs	UPF	812.11	556.74	0.183	29.13	-	40.49	25.87	34.11	59.51
	OPF	312.82	222.96	0.048	30	19.87	56.1	24.49	13.9	43.9
3 WTs	UPF	719.67	492.99	0.228	32.87	-	44.77	22.04	34.04	55.23
	OPF	214.44	153.64	0.065	32.87	20.35	60.41	21.54	13.35	39.59

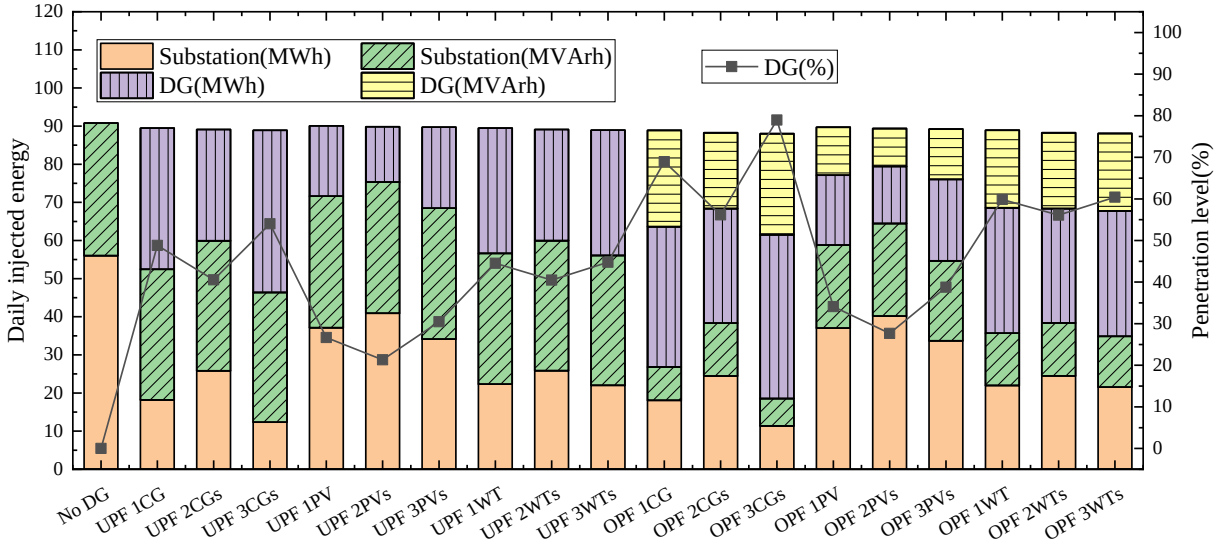

Fig. 24. Energy injection and DG penetration level for all cases in the 33-bus system

TABLE XIV
OPTIMAL CONFIGURATION SCHEME FOR DGS IN 69-BUS SYSTEM INCLUDING CGS, PVS, AND WTS)

		CG		PV		WT	
		DG size in kW (bus number)	*pf*	DG size in kW (bus number)	*pf*	DG size in kW (bus number)	*pf*
1 DG	UPF	1130.89(61)	1	1859.82(61)	1	3033.57(61)	1
	OPF	1114.43(61)	0.8149	1834.75(61)	0.8152	2989.54(61)	0.8149
2 DGs	UPF	320.6(17)	1	526.39(17)	1	859.99(17)	1
		1076.29(61)	1	1769.8(61)	1	2887.12(61)	1
	OPF	317.27(17)	0.8282	520.83(17)	0.8283	851.07(17)	0.8282
		1058.87(61)	0.814	1742.7(61)	0.8142	2840.48(61)	0.814
3 DGs	UPF	312(11)	1	514.007(11)	1	527.883(12)	1
		231.192(18)	1	378.766(18)	1	509.828(21)	1
		1039.092(61)	1	1709.281(61)	1	2716.138(61)	1
	OPF	300.279(11)	0.8137	491.368(11)	0.8142	539.316(12)	0.8013
		230.696(18)	0.8332	378.898(18)	0.8329	532.017(21)	0.8359
		1022.433(61)	0.814	1682.684(61)	0.8142	2682.494(61)	0.8139

The results show that, under constant or variable load and generation, the INGO algorithm proposed in this paper to allocate different DG types and power factors can effectively reduce the system's instantaneous power loss, daily energy loss, and voltage deviation, as well as improve the voltage distribution. In all cases, the results of the optimal configuration of the INGO algorithm proposed in this paper outperform the best results of the other compared algorithms. When replacing CGs with REDGs, PVs are less effective if the experiment time is 24 hours. The performance of WTs is not much different from CGs, so WTs can be chosen as REDGs to reduce carbon emissions.

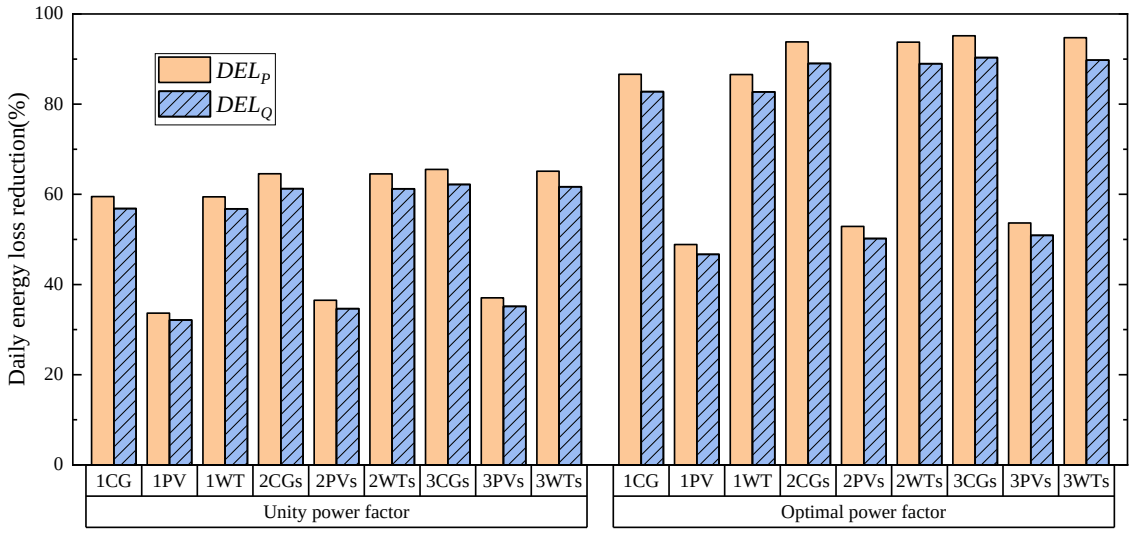

Fig. 25. Percentage reduction in daily energy loss for all configuration cases in the 69-bus system

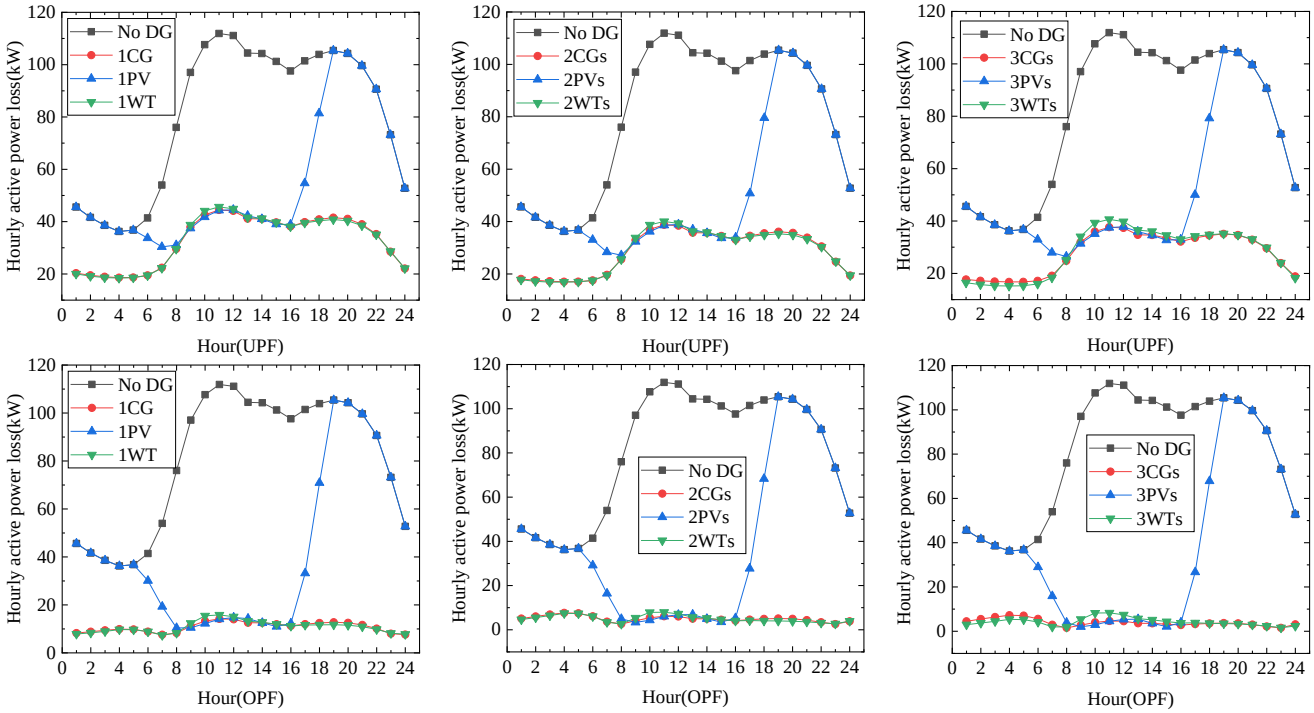

Fig. 26. Comparison of hourly active power loss in all configuration cases in the 69-bus system

TABLE XV
IMPACT OF THE OPTIMAL CONFIGURATION OF DIFFERENT DGS ON THE 69-BUS SYSTEM

DG number	*pf*	Energy loss		*DVD*	Energy from DG			Energy from Substation		
		kWh	kVArh		MWh	MVArh	*pl*(%)	MWh	MVArh	*pl*(%)
No DG	-	1936.65	882.55	0.857	-	-	-	57.247	40.183	100
1 CG	UPF	784.63	381.03	0.201	27.14	-	35.59	28.954	39.681	64.41
	OPF	258.94	152.01	0.128	26.75	19.03	48.17	28.819	20.422	51.83
2 CGs	UPF	686.09	341.89	0.08	33.53	-	42.39	22.466	39.642	57.61
	OPF	119.76	96.79	0.029	33.03	23.29	59.43	22.4	16.107	40.57
3 CGs	UPF	667.38	333.73	0.072	37.97	-	46.59	18.007	39.634	53.41
	OPF	93.9	85.47	0.026	37.28	26.33	67.14	18.124	13.055	32.86
1 PV	UPF	1285.07	598.93	0.487	13.51	-	18.7	43.085	39.899	81.3
	OPF	990.14	470.4	0.446	13.33	9.47	23.72	42.97	30.3	76.28
2 PVs	UPF	1229.73	576.95	0.419	16.68	-	22.83	39.86	39.877	77.17
	OPF	912.26	439.54	0.39	16.45	11.59	29.23	39.772	28.15	70.77
3 PVs	UPF	1219.19	572.36	0.415	18.9	-	25.64	37.629	39.872	74.36
	OPF	897.88	433.27	0.389	18.55	13.1	32.99	37.658	26.633	67.01
1 WT	UPF	785.45	381.39	0.201	27.11	-	35.55	28.985	39.681	64.45
	OPF	260.14	152.53	0.129	26.72	19	48.11	28.85	20.453	51.89
2 WTs	UPF	686.99	342.28	0.081	33.49	-	42.35	22.507	39.642	57.65
	OPF	121.06	97.35	0.029	32.99	23.26	59.36	22.441	16.137	40.64
3 WTs	UPF	675.38	338.29	0.095	33.548	-	42.41	22.437	39.638	57.59
	OPF	101.81	90.28	0.031	33.546	23.83	60.52	21.866	15.56	39.48

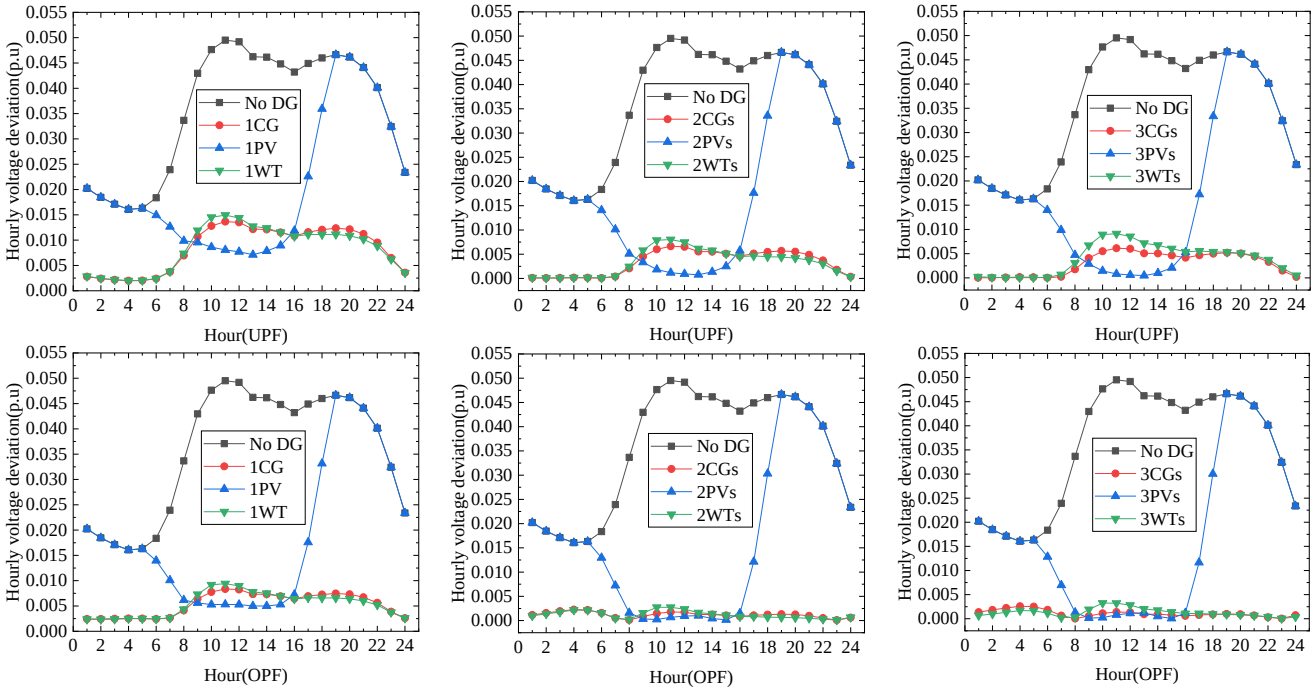

Fig. 27. Comparison of hourly voltage deviation in all configuration cases in the 69-bus system

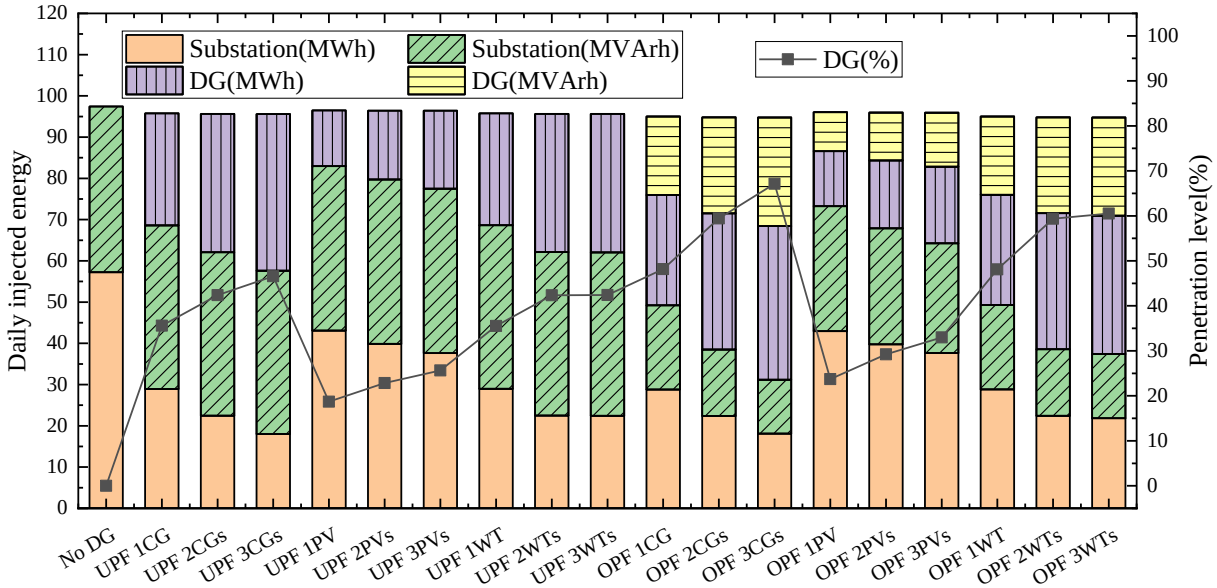

Fig. 28. Energy injection and DG penetration level for all cases in the 69-bus system

V. Conclusion

In this study, an INGO algorithm is proposed to simultaneously optimize the DGs' locations, capacities, and power factors in the DS to minimize instantaneous power loss, daily energy loss, and voltage deviation and improve penetration levels of REDGs and the voltage distribution. The following are the main conclusions drawn from this study.

Constant load and generation: For both the 33-bus and 69-bus RDNs, the simulation results of the INGO algorithm outperform the simulation results of the original NGO algorithm and other comparative literature, proving the effectiveness and stability of the INGO algorithm proposed in this paper. The DG running at optimal power factor gives better optimization results than the DG running at unity power factor, and the DG has a higher penetration level. The greater the number of DGs configured, the more significant the reduction in power loss and voltage deviation, and the more uniform the voltage distribution. The power loss reduction percentage in the 69-bus RDN is more significant than that in the 33-bus RDN, which indicates that the INGO algorithm has a more considerable advantage in solving ODGA problems with more control variables or more extensive search space.

Varied load and generation: The greater the number of DGs installed in the 33-bus and 69-bus test systems, the smaller the energy losses throughout the day. When the generators were at OPF, energy losses were even lower. In the 33-bus system, the DEL_P was reduced by 90.88%, 51.23%, and 88.27% when installing three CGs, PVs, and WTs operating at OPF, respectively. In the 69-bus system, the DEL_P was reduced by 95.15%, 53.64%, and 94.74%, respectively. It proves that the optimization framework proposed in this paper also has apparent advantages in solving the dynamic ODGA problem. The more complex the

dynamic model is, the better the results are. WTs significantly outperform PVs in reducing all-day energy losses and voltage deviations, with very little difference from CGs. However, if we consider only the period of high light intensity, from 8:00 to 16:00, PVs outperform WTs, even with lower voltage deviation than CGs. If the period under consideration is 24 hours, WTs can be chosen instead of CGs to reduce energy loss and carbon emissions throughout the day. If the period under consideration is from 8:00 to 16:00, PVs should be selected as REDGs.

The results show that the locations, capacities, power factors, and types of DGs are essential in the optimal configuration of DGs. If allocated properly, they can significantly reduce the instantaneous power loss, daily energy loss, and voltage deviation of the system, mitigate the greenhouse effect, and improve the system's voltage distribution and reliability.

REFERENCES

[1] G. Chen, J. Qian, Z. Zhang, and Z. Sun, "Multi-objective improved bat algorithm for optimizing fuel cost, emission and active power loss in power system," *IAENG International Journal of Computer Science*, vol. 46, no. 1, pp. 118-133, 2019.

[2] S. Ghosh, S. P. Ghoshal, and S. Ghosh, "Optimal sizing and placement of distributed generation in a network system," *International Journal of Electrical Power & Energy Systems*, vol. 32, no. 8, pp. 849-856, 2010.

[3] X. Yuan, C. Chen, M. Jiang, and Y. Yuan, "Prediction interval of wind power using parameter optimized Beta distribution based LSTM model," *Applied Soft Computing*, vol. 82, article. 105550, 2019.

[4] P. G. Mccormick and H. Suehrcke, "The effect of intermittent solar radiation on the performance of PV systems," *Solar Energy*, vol. 171, pp. 667-674, 2018.

[5] R. Shah, N. Mithulananthan, R. C. Bansal, and V. K. Ramachandaramurthy, "A review of key power system stability challenges for large-scale PV integration," *Renewable and Sustainable Energy Reviews*, vol. 41, pp. 1423-1436, 2015.

[6] D. Q. Hung, N. Mithulananthan, and R. C. Bansal, "Analytical strategies for renewable distributed generation integration considering energy loss minimization," *Applied Energy*, vol. 105, pp. 75-85, 2013.

[7] P. Kayal, S. Chanda, and C. K. Chanda, "An analytical approach for allocation and sizing of distributed generations in radial distribution network," *International Transactions on Electrical Energy Systems*, vol. 27, no. 7, article. 2322, 2017.

[8] S. Sultana and P. K. Roy, "Krill herd algorithm for optimal location of distributed generator in radial distribution system," *Applied Soft Computing*, vol. 40, pp. 391-404, 2016.

[9] A. M. Shaheen, A. M. Elsayed, R. A. El-Sehiemy, and A. Y. Abdelaziz, "Equilibrium optimization algorithm for network reconfiguration and distributed generation allocation in power systems," *Applied Soft Computing*, vol. 98, article. 106867, 2021.

[10] E. Mahboubi-Moghaddam, M. R. Narimani, and M. H. Khooban *et al.*, "Multi-objective distribution feeder reconfiguration to improve transient stability, and minimize power loss and operation cost using an enhanced evolutionary algorithm at the presence of distributed generations," *International Journal of Electrical Power & Energy Systems*, vol. 76, pp. 35-43, 2016.

[11] T. H. B. Huy, T. V. Tran, D. N. Vo, and H. T. T. Nguyen, "An improved metaheuristic method for simultaneous network reconfiguration and distributed generation allocation," *Alexandria Engineering Journal*, vol. 61, no. 10, pp. 8069-8088, 2022.

[12] G. Chen, A. Zhang, C. Zhao, and Z. Zhang, "Optimal placement and capacity of combined DGs and SCs in radial distribution networks based on PSO-OS algorithm," *IAENG International Journal of Computer Science*, vol. 48, no. 2, pp. 236-249, 2021.

[13] G. Chen, X. Zhao, and K. Peng *et al.*, "Optimized configuration of location and size for DGs and SCs in radial distributed networks based on improved butterfly algorithm," *IAENG International Journal of Applied Mathematics*, vol. 52, no. 1, pp. 81-100, 2022.

[14] R. Palanisamy and S. K. Muthusamy, "Optimal siting and sizing of multiple distributed generation units in radial distribution system using ant lion optimization algorithm," *Journal of Electrical Engineering & Technology*, vol. 16, no. 1, pp. 79-89, 2021.

[15] S. Nagaballi and V. S. Kale, "Pareto optimality and game theory approach for optimal deployment of DG in radial distribution system to improve techno-economic benefits," *Applied Soft Computing*, vol. 92, article. 106234, 2020.

[16] S. Cheng, M. Chen, and P. J. Fleming, "Improved multi-objective particle swarm optimization with preference strategy for optimal DG integration into the distribution system," *Neurocomputing*, vol. 148, pp. 23-29, 2015.

[17] S. Kumar, K. K. Mandal, and N. Chakraborty, "Optimal DG placement by multi-objective opposition based chaotic differential evolution for techno-economic analysis," *Applied Soft Computing*, vol. 78, pp. 70-83, 2019.

[18] N. K. Meena, A. Swarnkar, N. Gupta, and K. R. Niazi, "Multi-objective Taguchi approach for optimal DG integration in distribution systems," *IET Generation, Transmission & Distribution*, vol. 11, no. 9, pp. 2418-2428, 2017.

[19] B. Poornazaryan, P. Karimyan, G. B. Gharehpetian, and M. Abedi, "Optimal allocation and sizing of DG units considering voltage stability, losses and load variations," *International Journal of Electrical Power & Energy Systems*, vol. 79, pp. 42-52, 2016.

[20] G. Chen, S. Li, and H. Long *et al.*, "A hybrid algorithm introducing cross mutation and non-linear learning factor for optimal allocation of DGs and minimizing annual network loss in the distribution network," *IAENG International Journal of Applied Mathematics*, vol. 51, no. 3, pp. 569-586, 2021.

[21] M. Pesaran H. A., M. Nazari-Heris, B. Mohammadi-Ivatloo, and H. Seyedi, "A hybrid genetic particle swarm optimization for distributed generation allocation in power distribution networks," *Energy*, vol. 209, article. 118218, 2020.

[22] M. H. Moradi and M. Abedini, "A combination of genetic algorithm and particle swarm optimization for optimal DG location and sizing in distribution systems," *International Journal of Electrical Power & Energy Systems*, vol. 34, no. 1, pp. 66-74, 2012.

[23] A. S. Hassan, Y. Sun, and Z. Wang, "Multi-objective for optimal placement and sizing DG units in reducing loss of power and enhancing voltage profile using BPSO-SLFA," *Energy Reports*, vol. 6, pp. 1581-1589, 2020.

[24] H. M. H. Farh, A. M. Al-Shaalan, A. M. Eltamaly, and A. A. Al-Shamma'a, "A novel severity performance index for optimal allocation and sizing of photovoltaic distributed generations," *Energy Reports*, vol. 6, pp. 2180-2190, 2020.

[25] S. Kansal, V. Kumar, and B. Tyagi, "Hybrid approach for optimal placement of multiple DGs of multiple types in distribution networks," *International Journal of Electrical Power & Energy Systems*, vol. 75, pp. 226-235, 2016.

[26] T. P. Nguyen, T. A. Nguyen, T. V. Phan, and D. N. Vo, "A comprehensive analysis for multi-objective distributed generations and capacitor banks placement in radial distribution networks using hybrid neural network algorithm," *Knowledge-Based Systems*, vol. 231, article. 107387, 2021.

[27] T. L. Duong, P. T. Nguyen, N. D. Vo, and M. P. Le, "A newly effective method to maximize power loss reduction in distribution networks with highly penetrated distributed generations," *Ain Shams Engineering Journal*, vol. 12, no. 2, pp. 1787-1808, 2021.

[28] D. B. Prakash and C. Lakshminarayana, "Multiple DG placements in radial distribution system for multi objectives using Whale Optimization Algorithm," *Alexandria Engineering Journal*, vol. 57, no. 4, pp. 2797-2806, 2018.

[29] A. Eid, "Allocation of distributed generations in radial distribution systems using adaptive PSO and modified GSA multi-objective optimizations," *Alexandria Engineering Journal*, vol. 59, no. 6, pp. 4771-4786, 2020.

[30] K. H. Truong, P. Nallagownden, I. Elamvazuthi, and D. N. Vo, "An improved meta-heuristic method to maximize the penetration of distributed generation in radial distribution networks," *Neural Computing and Applications*, vol. 32, no. 14, pp. 10159-10181, 2020.

[31] S. K. Dash, S. Mishra, and A. Y. Abdelaziz *et al.*, "Optimal allocation of distributed generators in active distribution networks using a new oppositional hybrid sine cosine muted differential evolution algorithm," *Energies*, vol. 15, no. 6, article. 2267, 2022.

[32] D. Q. Hung, N. Mithulananthan, and K. Y. Lee, "Determining PV penetration for distribution systems with Time-Varying load models," *IEEE Transactions on Power Systems*, vol. 29, no. 6, pp. 3048-3057, 2014.

[33] H. Yi, M. H. Hajiesmaili, and Y. Zhang *et al.*, "Impact of the uncertainty of distributed renewable generation on deregulated electricity supply chain," *IEEE Transactions on Smart Grid*, vol. 9, no. 6, pp. 6183-6193, 2018.

[34] Z. Ullah, S. Wang, and J. Radosavljević, "A novel method based on PPSO for optimal placement and sizing of distributed generation," *IEEJ Transactions on Electrical and Electronic Engineering*, vol. 14, no. 12, pp. 1754-1763, 2019.

[35] P. D. Huy, V. K. Ramachandaramurthy, and J. Y. Yong *et al.*, "Optimal placement, sizing and power factor of distributed generation: A comprehensive study spanning from the planning stage to the operation stage," *Energy*, vol. 195, article. 117011, 2020.

[36] M. Dehghani, S. Hubalovsky, and P. Trojovsky, "Northern goshawk optimization: A new Swarm-Based algorithm for solving optimization problems," *IEEE Access*, vol. 9, pp. 162059-162080, 2021.

[37] M. M. Aman, G. B. Jasmon, A. H. A. Bakar, and H. Mokhlis, "Optimum network reconfiguration based on maximization of system loadability using continuation power flow theorem," *International Journal of Electrical Power & Energy Systems*, vol. 54, pp. 123-133, 2014.

[38] H. Manafi, N. Ghadimi, M. Ojaroudi, and P. Farhadi, "Optimal placement of distributed generations in radial distribution systems using various PSO and DE algorithms," *Electronics and Electrical Engineering*, vol. 19, no. 10, pp. 53-57, 2013.

[39] S. K. Sudabattula, "Optimal allocation of solar based distributed generators in distribution system using Bat algorithm," *Perspectives in Science*, vol. 8, pp. 270-272, 2016.

[40] S. Velamuri, S. H. C. Cherukuri, and S. K. Sudabattula *et al.*, "Combined approach for power loss minimization in distribution networks in the presence of gridable electric vehicles and dispersed generation," *IEEE Systems Journal*, vol. 16, no. 2, pp. 3284-3295, 2022.

[41] S. Elsaiah, M. Benidris, and J. Mitra, "Analytical approach for placement and sizing of distributed generation on distribution systems," *IET Generation, Transmission & Distribution*, vol. 8, no. 6, pp. 1039-1049, 2014.

[42] M. M. Aman, G. B. Jasmon, A. H. A. Bakar, and H. Mokhlis, "A new approach for optimum simultaneous multi-DG distributed generation Units placement and sizing based on maximization of system loadability using HPSO (hybrid particle swarm optimization) algorithm," *Energy*, vol. 66, pp. 202-215, 2014.

[43] D. Q. Hung and N. Mithulananthan, "Multiple distributed generator placement in primary distribution networks for loss reduction," *IEEE Transactions on Industrial Electronics*, vol. 60, no. 4, pp. 1700-1708, 2013.

[44] A. Selim, S. Kamel, A. S. Alghamdi, and F. Jurado, "Optimal placement of DGs in distribution system using an improved harris hawks optimizer based on single- and multi-Objective approaches," *IEEE Access*, vol. 8, pp. 52815-52829, 2020.

[45] R. J. Mahfoud, Y. Sun, and N. F. Alkayem *et al.*, "A novel combined evolutionary algorithm for optimal planning of distributed generators in radial distribution systems," *Applied Sciences*, vol. 9, no. 16, article. 3394, 2019.

[46] N. Jain, S. N. Singh, and S. C. Srivastava, "A generalized approach for DG planning and viability analysis under market scenario," *IEEE Transactions on Industrial Electronics*, vol. 60, no. 11, pp. 5075-5085, 2013.

[47] K. Mahmoud, N. Yorino, and A. Ahmed, "Optimal distributed generation allocation in distribution systems for loss minimization," *IEEE Transactions on Power Systems*, vol. 31, no. 2, pp. 960-969, 2016.

[48] S. Sultana and P. K. Roy, "Multi-objective quasi-oppositional teaching learning based optimization for optimal location of distributed generator in radial distribution systems," *International Journal of Electrical Power & Energy Systems*, vol. 63, pp. 534-545, 2014.

[49] E. H. M. E. Abu-Mouti, "Heuristic curve-fitted technique for distributed generation optimisation in radial distribution feeder systems," *IET Generation, Transmission & Distribution*, vol. 5, no. 2, pp. 172-180, 2011.

[50] M. Purlu and B. E. Turkay, "Optimal allocation of renewable distributed generations using heuristic methods to minimize annual energy losses and voltage deviation index," *IEEE Access*, vol. 10, pp. 21455-21474, 2022.